Available online at www.sciencedirect.com

SciVerse ScienceDirect

journal homepage: www.elsevier.com/locate/he

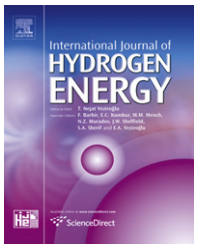

# A rigorous computational model for hydrogen production from bio-ethanol to feed a fuel cell stack

*Lucas Nieto Degliuomini* [a,b], *Sebastian Biset* [a,c], *Patricio Luppi* [a,b], *Marta S. Basualdo* [a,b,c,*]

[a] *Computer Aided for Process Engineering Group (CAPEG), Av. 27 de Febrero, 210 bis, CP S2000EZP, Rosario - Santa Fe, Argentina*
[b] *French-Argentine International Center of Information and Systems Science- CONICET-UNR-UPCAM, Av. 27 de Febrero, 210 bis, CP S2000EZP, Rosario - Santa Fe, Argentina*
[c] *Technological National University - Faculty of Rosario -(UTN-FRRo), Zeballos 1341 - S2000BQA, Rosario - Santa Fe, Argentina*

ARTICLE INFO

*Article history:*
Received 15 July 2011
Received in revised form
27 September 2011
Accepted 1 October 2011
Available online 20 December 2011

*Keywords:*
Bio-ethanol processor
PEM
Rigorous dynamic model
Hydrogen generation

ABSTRACT

A pseudo dynamic rigorous model of a bio-ethanol processor system (BPS) to produce hydrogen for feeding a Proton Exchange Membrane Fuel Cell (PEM-FC) is presented. The main contribution of this work is to give the overall set of differential and algebraic equations (DAE), assumptions and the way to computationally implement it. This model is able for testing the dynamic behavior of this integrated process, obtaining a reduced order linear model and checking any plant-wide control structure design. It is implemented in two programs, HYSYS and MATLAB, properly communicated to coordinate the calculations performed on each one. A part of the process considered with a faster dynamic than the rest of the units of the plant are simulated in HYSYS environment working in steady state mode. Then, auxiliary equipments and the heat exchangers network are in HYSYS which is called by MATLAB every integration interval for doing the simulation of the complete system. On the other side, the PEM-FC and the dynamic models of the plug flow reactors are developed in MATLAB workspace. Hence, strictly speaking this model must be considered as "pseudo" dynamic. The linearized and reduced order model is developed by applying system identification techniques on the rigorous model. Therefore, accounting the main objectives of the process and the most critical disturbances, a preliminary control structure can be well-tested here. Several results are presented in this work analyzing the obtained performances for opened and closed loop modes.


## 1. Introduction

The various difficulties and risks involved in storage, distribution, and refueling of hydrogen makes fuel processors the best way to feed Fuel Cells (FC). Natural gas and gasoline are common fuels considered as sources of energy for FC. However, they generate $CO_2$ during their combustion which goes into the atmosphere and contributes to the environment pollution. Other sources are methanol and ethanol which can be obtained from renewable feedstocks or agriculture residues. Hence, the produced $CO_2$ will be consumed by biomass growth, offering a nearly closed carbon loop. This cycle is very important to be considered since currently, the restrictions to prevent the continuous growth of environmental degradation

* *Corresponding author*. CIFASIS, French-Argentine International Center of Information and Systems Science- CONICET-UNR-UPCAM, Av. 27 de Febrero, 210 bis, CP S2000EZP, Rosario - Santa Fe, Argentina. Tel.: +54 341 423 7248; fax: +54 341 482 1772.
E-mail addresses: nieto@cifasis-conicet.gov.ar (L. Nieto Degliuomini), sbiset@frro.utn.edu.ar (S. Biset), luppi@cifasis-conicet.gov.ar (P. Luppi), basualdo@cifasis-conicet.gov.ar (M.S. Basualdo).
0360-3199/$ – see front matter 
doi:10.1016/j.ijhydene.2011.10.069

has become a matter of vital importance, mainly due to the consequences of global warming. One of the biggest contributors to this situation is the vehicular traffic, the major consumer of fossil fuel.

During the last decades, the need for obtaining more efficient processes and improve benefits has been growing exponentially. In this new millennium, the main focus is pointed to improvements in energy efficiencies. In this context, the fuel cell, feeded by hydrogen, represents an excellent alternative because they have higher efficiency with respect to internal combustion engines and its environmental friendliness, since water and heat are the only emissions. Transportation based on hydrogen from renewable sources represents an enormous improvement for the global economy, replacing the dangerous dependence on fossil fuels, as stated in [1]. Among the Fuel Cells, the Proton Exchange Membrane (PEM-FC) is best suited to the requirements of portability of a mobile system and is capable of working at relatively low temperatures [2].

The ideal situation for a Fuel Cell would be to be fed with pure Hydrogen, which carries many issues of implementation. From the lack of infrastructure to produce and distribute enough amounts of Hydrogen to the difficulties and dangers of transport and storage it. To overcome these difficulties, several solutions have been proposed, one of them is the operation of Cells able to be fed directly with gasoline or diesel fuel, but sacrificing efficiency. The most plausible solution, that concerns this work, is to process a fuel onboard to produce a Hydrogen rich synthesis gas. Bio-ethanol is the best candidate to be the fuel of tomorrow, since it does not have the toxicity of methanol. Both of them are relatively easy and cheap to produce, although methanol has a more beneficial H/C ratio. Applying an energy balance to bio-ethanol, a positive net value is achieved accounting the relationship between the obtained energy from its combustion respect to that required for its production. The energy to obtain bio-ethanol, means the entire cycle of life since raw materials extraction, required inputs, transport, up to the process of transformation. The value of this relation has been stated by Sanchez and Cardona [3] equal to 8 for the production from sugar cane, and 6 from lignocellulosic residue materials. Obviously, if it is compared with fossil fuels, that can achieve values between 10 and 23 [4], is a poor fuel. But of course, the energy required to recapture $CO_2$ and turn it into a hydrocarbon again is enormous and would turn the balance into a small fraction. Economic analysis for the production of hydrogen from bio-ethanol in America are presented in [5] and [6], for the cases of United States and Argentina respectively. These works actually consider the industrial scale production, a deeper survey on this subject can be seen in [7].

Usual methods of converting bio-ethanol are catalytic partial oxidation and steam reforming. This last one is considered because high concentrations of hydrogen can be obtained to feed the fuel cell stack. A complete survey on the current literature for ethanol steam reforming can be seen in [8]. They investigated on Cerium–Nickel mixed oxide catalysts, over a wide range of parameters and presented results on hydrogen storage by chemical titration. An energy efficiency analysis for the production of hydrogen by the bio-ethanol steam reforming reaction is presented in [9], along with a comparison with the obtention via Pd-Ag membrane processes.

In this work to develop the catalytic plug flow reactor models as stage-wise unit operations the book of [10] was accounted.

The efficiency of the processor can be improved by considering an energetically integrated system by reutilizing the heat contained in the flows. The main objective is to keep the process in optimal operating conditions. The heat exchange is not a trivial task specially when a great number of operating units are involved. Recently, Oliva et al. [11] presented a deep analysis in the configuration of the heat exchangers network, and a novel methodology to synthesize it.

Dynamic models reveal much information about performance and they are specially needed for evaluating transient responses when changes on operating points or disturbances affect the system. Dynamic rigorous models of fuel cell power plants are extremely important for understanding the interactions among the variables, implications on system performance and transient behaviors, hardly analyzed nowadays. When a dynamic model is available since the plant design stage gives the opportunity of analyzing the temporal behavior around a specific operating point which generally is adopted based on efficiency considerations. The development of a dynamic model for a gasoline processor is described in [12]. They validated the model and estimated the parameters with the obtained measures from a 4 kW fuel processor test bench. Pd-Ag membrane methanol loop reactors are analyzed in [13]. They present a detailed dynamic model, and then compare it to a conventional model, validated against plant data. Koc et al. [14] developed a dynamic modeling framework for characterizing the transient behavior of a WGS membrane reactor. They also propose some control ideas in order to enhance the performance of the reactor against unusual events such as the presence of disturbances or plant start-up. A control-oriented model of a catalytic partial oxidation of natural gas processor using physics-based principles was developed in [15]. They guided the control design of the fuel processor system (FPS) combined with a PEM-FC employing control theoretic tools [16]. Highlighted major issues of FPS control, that is regulating the amount of hydrogen in the fuel cell anode and the temperature of the catalytic partial oxidation reactor during transient power demands from the FC. The limitations of a decentralized controller and the benefits of a multivariable controller were identified by [17] using linear and feedback analysis. A mathematical model of the reformer is developed by [18] and selected parameters of the model were fit to match experimental data from the dynamic response of the process. Then they designed a reformer with as minimum as possible combined volume of the steam reformer and WGS reactors.

According to the review given above, can be considered that this work is one of the first that deals with a pseudo dynamic model of a complete and energetically integrated fuel processor system with a PEM-FC where bio-ethanol is the raw material. The construction of this model is based on three main sources [19], [20] and [21]. The definition of the best operating point for the process was obtained from the pioneer work of [19], who performed the synthesis of the complete process in steady state using HYSYS environment. Hence, the

pseudo dynamic model is based on the efficiency considerations and dimensions given in that work which results were previously checked. Thanks to the use of that first steady state model it was possible to define in [21] the most critical control loops via sensitivity analysis. Therefore, this paper can be considered as a continuation of these last two works. Additionally, the dynamic model of the PEM-FC was taken from the book of [20] and included in the model of the overall system presented here.

Then, to explain the different steps of the model building, since the DAE up to its computational implementation the following sections are included: in Section 2 the fuel processor system with its reactors is described. Section 3 presents a short discussion about the main characteristics of the PEM-FC. In Section 4 a brief description about how is handled the MATLAB/HYSYS interface is performed. Then, in Section 4.1 the part of the model implemented in HYSYS is detailed, mainly because the heat exchanger network is solved by the 'LNG' tool. Several tests were done with the model to check the assumptions consistency. Next, considering this model helpful to design control structures in Section 5 the use of the rigorous model for obtaining a reduced order and linearized dynamic model via system identification techniques is discussed. In Section 6 the control structure implemented accounting objectives and sensitivity analysis is shown. In Section 7 the simulation results including the model validation, the obtained state-space linearized model and the tests of the control structure design are included. Finally, in Section 8 conclusions and some proposed future works are presented.

## 2. Bio-ethanol processor system

The BPS analyzed in this work is illustrated in Fig. 1. It consists of an Ethanol Steam Reforming (ESR) plug flow reactor, where most of the conversion of ethanol to $H_2$ is made. Carbon monoxide (CO) which poisons the fuel cell catalyst is produced in the ESR, so additional processing is needed to remove this substance. There are three reactors that configure the cleaning system; these are two Water Gas Shift, one of high temperature (fast), and the other of low temperature, that favors the equilibrium of the reaction to higher conversion rates of CO. The third is a Preferential Oxidation of Carbon monoxide (CO-PrOx) reactor, where oxidation of CO into $CO_2$ is produced. However, the undesired oxidation of $H_2$ may occur too, so the catalyst is selected to promote mainly the conversion of CO.

Ethanol and vaporized water are mixed and then supplied to the ESR reactor, where the following endothermic reaction occur:

$$(\mathrm{ESR})\ CH_3CH_2OH + H_2O \leftrightarrow H_2 + CO_2 + CO + CH_4 + CH_3CHO$$

The heat requirement is supplied by hot gases provided by the burner which are fed to the jacket of the reformer. The water gas shift reaction is produced in both WGS reactors operating at different temperatures, it is given by:

$$(\mathrm{WGS})\ CO + H_2O \leftrightarrow CO_2 + H_2$$

This reaction produces heat and generates more hydrogen. However the levels of CO are still high even after the two WGS reactors. So the final elimination is made in the CO-PrOx reactor, which produces the oxidation of CO into $CO_2$ and the undesired combustion of $H_2$:

$$(CO - Ox)CO + \frac{1}{2}O_2 \leftrightarrow CO_2$$

$$(H_2 - Ox)\ H_2 + \frac{1}{2}O_2 \leftrightarrow H_2O$$

The WGS reaction takes place in this reactor too. Oxygen is injected into the CO-PrOx, the amount needed is about twice the stoichiometric magnitude to have a good selectivity and satisfy the requirements of the FC.

In the case analyzed here, plug flow (PFR) reactors are modeled according to the recommendations of experimental works. Since the conditions inside these reactors vary along the distance and in time, they should be strictly modeled by partial differential equations. An alternative way of solving them is discretizing the model, considering a lumped configuration. The reactor is divided in a proper number of slices, assuming that each one of them works as a continuous stirred tank reactor (CSTR). Hence, a series of these reactors, space independent and with homogeneous conditions inside, allows to model the system by means of ordinary differential equations.

Under this assumption, the total mass balance can be written in the following manner:

$$\frac{d(n_t)}{dt} = Fr_{in} - Fr_{out} + \left[\sum_{j,i} \nu_{j,i} \cdot (-r_i)\right] \cdot w_{cat}, \quad (1)$$

where $n_t$ is the total number of moles for each slice, $Fr_{in}$ and $Fr_{out}$ are input and output molar flows, $\nu_{j,i}$ is the stoichiometric coefficient for the component $j$ in reaction $i$, $(-r_i)$ is the reaction rate and $w_{cat}$ is the total catalyst mass involved in this reactor. $w_{cat}$ plays the role of the reactor volume, but since this is a catalyzed reaction, and the reaction rate is given by the mass of catalyst, the weight portion is included in the differential equation. Additionally, the pressure variation for each slice $\Delta P$ is neglected, ideal gases behavior is considered. Then, the variation in time ($t$) of the total number of moles in each

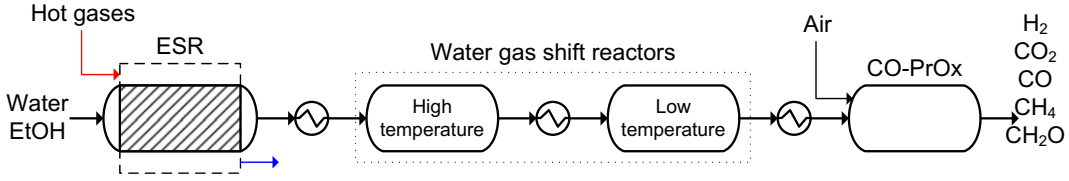


**Fig. 1 – Bio-ethanol processor system.**

slice is neglected, hence $d(n_t)/dt$ is equal to zero. Under this consideration the exit flow can be determined algebraically. Therefore, considering the component mass balance, the term $d(n_t \cdot y_j)/dt$, can be written as $n_t \cdot d(y_j)/dt$ and calculated through the following general expression:

$$\frac{d\left(y_j\right)}{dt} = \frac{Fr_{in} \cdot y_{j,in} - Fr_{out} \cdot y_j + \left[\sum_i \nu_{j,i} \cdot (-r_i)\right] \cdot w_{cat}}{n_t}, \quad (2)$$

where $y_j$ is the molar fraction of component $j$. Each of the involved reactions assume the following general kinetic expression:

$$(-r_i) = k_i \cdot \exp\left(-\frac{E_i}{R_g \cdot T}\right) \cdot \left(\prod_{j=1}^{Rc} y_j^{\nu_{j,i}} - \frac{\prod_{j=1}^{Pr} y_j^{\nu_{j,i}}}{K_{eq,i}}\right). \quad (3)$$

It is based in the molar fractions of the substances ($y_j$) where $\nu_j^i$ represents the stoichiometric coefficient of component $j$ in reaction $i$. $Pr$ represents the number of products and $R_c$ the reactants, $k_i$ is calculated from Arrhenius law as a temperature function. For each reaction the frequency factor ($k_i$) and activation energy ($E_i$) must be specified. The expression of the equilibrium constant for each reaction ($K_{eq,i}$) is determined with the variation of the Gibbs free energy.

From the energy balance the temperature variation is obtained as follows:

$$\frac{d(T)}{dt} = \frac{Fr_{in} \cdot cp_{in} \cdot T_{in} - Fr_{out} \cdot cp \cdot T + \left[\sum_i \nu_{j,i} \cdot (-\Delta H_i) \cdot (-r_i)\right] \cdot w_{cat} + Q}{n_t \cdot cp}, \quad (4)$$

where $T$ is the temperature of each slice, $cp$ is the specific heat of the stream, $(-\Delta H)$ is the heat of reaction and $Q$ is the exchanged heat. This term is neglected in all the adiabatic reactors. Only in the case of the ESR $Q$ must be accounted. The heat of reaction depends of the temperature according to:

$$\Delta H_i = \sum_j \nu_{j,i} \cdot \Delta H_{f,j}^0 + \int_{T^0}^{T} \left(\sum_j \nu_{j,i} \cdot cp_j^0\right) dT, \quad (5)$$

where $cp_j^0$ is the specific heat of component $j$ and $\Delta H_{f,j}^0$ the formation heat of component $j$ at reference temperature $T^0$. The calculation of $cp_j^0$ is based on the data provided by [22].

### 2.1. Ethanol steam reforming

The stoichiometric reaction for hydrogen production was given at Section 2 identified by (ESR). Despite the apparent simplicity of this reaction it must be remarked that it involves a complex system of reactions, and the selectivity for $H_2$ product is affected by a number of undesired secondary reactions. The reforming of ethanol is feasible for temperatures higher than 230 °C.

The analysis made by [23] adjusting experimental data of a Cobalt catalyst supported in Zircon ($CO/ZrO_2$), leads to the reaction scheme of acetaldehyde decomposition, according to the mechanism proposed by [24]:

Reaction A $CH_3CH_2OH \leftrightarrow CH_3CHO + H_2$ $\Delta H_{298K}^A = -70.6\,kJ/mol$

Reaction B $CH_3CHO \leftrightarrow CO + CH_4$ $\Delta H_{298K}^B = -21.9\,kJ/mol$

Reaction C $CH_4 + H_2O \leftrightarrow CO + 3 \cdot H_2$ $\Delta H_{298K}^C = 205.9\,kJ/mol$

Reaction D $CO + H_2O \leftrightarrow CO_2 + H_2$ $\Delta H_{298K}^D = -41.18\,kJ/mol$

To achieve a good yield it is necessary to operate at a high temperature (>550 °C).

Since the plug flow reactor is modeled as a number of sequenced CSTR, all mass and energy balances are made over each one with the same assumptions given above. A detailed description of the mass and energy balances with the necessary auxiliary calculations is presented in the Appendix.

Some preliminary simulations were done without considering any perturbation to check model consistency. In Section 7.1 the obtained profiles for the reforming reactor can be observed.

### 2.2. Water gas shift

In these reactors, the only reaction that takes place is the WGS, it is widely used in the industry in ammonia synthesis and hydrogen production by means of hydrocarbon reforming. The reaction scheme is:

Reaction WGS $CO + H_2O \leftrightarrow CO_2 + H_2$ $\Delta H_{298K}^{WGS} = -41.18\,kJ/mol$

The main objectives of the WGS reaction are to remove the CO from streams and adjust the $H_2$/CO molar ratio. This reaction is moderately exothermic and its equilibrium constant decreases as temperature rises, so lower temperature favors high conversions. These process units belong to the cleaning system and work adiabatically. This condition can limit their performance, so is better to consider more than one WGS reactor with intermediate cooling. The mass and energy balances for the WGS reactors can be seen in the Appendix. In this work, the reactors are considered adiabatic, in order to obtain the best efficiency for the system. If heat losses are accounted, then the energy balances are affected and the efficiency reduced. Then the system is forced to be adiabatic to get the upper bound for the performance.

#### 2.2.1. High temperature WGS

The first is the High Temperature water gas Shift (HTS) reactor. It uses an iron based catalyst (Fe/Cr) that operates between 300 °C and 550 °C, and makes most of the conversion of CO.

Kinetic parameters used in this work for the HTS reactor are given by [25]. They adjusted the reaction data (industrial conditions) for an iron based catalyst and proposed a power law expression as:

$$r_{WGS} = 1.197 \cdot 10^3 \cdot \exp\left(-\frac{78213}{R_g \cdot T}\right) \cdot C_{CO}^{0.73} \cdot C_{H_2O}^{0.55} - 9.0919 \cdot 10^4 \cdot \exp\left(-\frac{116270}{R_g \cdot T}\right) \cdot C_{CO}^{-0.27} \cdot C_{H_2O}^{-0.45} \cdot C_{CO_2} \cdot C_{H_2} \quad (6)$$

Where $C_j$ is the concentration of component $j$ (CO, $H_2O$, $CO_2$ and $H_2$).

#### 2.2.2. Low temperature WGS

The Low Temperature water gas Shift (HTS) reactor operates at lower temperatures (150 °C – 230 °C) and uses a Copper–Zinc catalyst supported over Alumina, its composition is usually $CuO/ZnO/Al_2O_3$. However, it is sensitive to poisoning by Chlorides and Sulfurs. The WGS reaction is thermodynamically favored, so higher conversion rates are obtained since the equilibrium constant is low.

The kinetic expression obtained by [26] is used. They determined the parameters under the most likely conditions for a methanol reforming reactor, that is composition and pressures, which are similar to the ethanol processor under study here. They used a Süd-Chemie commercial available catalyst and provide the following expression:

$$r_{WGS} = 82.2 \cdot \exp\left(-\frac{47400}{R_g \cdot T}\right) \cdot \left(P_{CO} \cdot P_{H_2O} - \frac{P_{CO_2} \cdot P_{H_2}}{K_{eq}}\right) \quad (7)$$

Where $K_{eq}$ represents the equilibrium constant, which can be calculated with the following equation provided by Chinchen et al. ([26]):

$$\ln(K_{eq}) = \frac{5693.5}{T} + 1.077 \cdot \ln(T) + 5.44 \cdot 10^{-4} \cdot T - 1.125 \cdot 10^{-7} \cdot T^2 - \frac{49170}{T^2} - 13.148 \quad (8)$$

### 2.3. Preferential oxidation of carbon monoxide

The feed stream to the FC must have only small amounts of CO. Therefore, the last reactor needed to complete the cleaning system is the Preferential Oxidation of Carbon Monoxide (CO-PrOx) reactor. The main (desired) reaction given in this stage is the oxidation of CO into $CO_2$. However, the undesirable oxidation of $H_2$ is produced too, causing an efficiency reduction of the FPS and temperature increasing. It has been reported by [27] that WGS type reaction should be considered at this stage. For the CO-PrOx the reactions are:

Reaction WGS $\quad CO + H_2O \leftrightarrow CO_2 + H_2 \quad \Delta H^{WGS}_{298K} = -41.18$ kJ/mol

Reaction E $\quad CO + \frac{1}{2}O_2 \leftrightarrow CO_2 \quad \Delta H^{E}_{298K} = -283$ kJ/mol

Reaction F $\quad H_2 + \frac{1}{2}O_2 \leftrightarrow H_2O \quad \Delta H^{F}_{298K} = -242$ kJ/mol

In the Appendix, the mass and energy balances are shown for the CO-PrOx reactor. In Section 7.1 the resulting profiles for the reforming reactor and cleaning system can be seen.

### 2.4. Burner

The necessary heat for producing the reactions at the ESR is obtained by burning the mix of ethanol and air at the burner. This stage is very important to reach good yields. Then, in this equipment, hot gases are generated and will go to the jacket of the ESR. Hence, in this unit, a complete combustion of all the ethanol that is fed can be assumed provided that the stoichiometric amount of oxygen is given. It means that the amount of ethanol reacting ($EtOH_{react}$) is equal to its input flow. In addition, the exit gases from the PEM-FC are fed into this reactor to burn completely the remaining ethanol and methane. This unit is modeled as an adiabatic and continuous stirred tank reactor (CSTR) in HYSYS environment. The reactions taking place in this equipment are:

$CH_3CH_2OH + 3 \cdot O_2 \rightarrow 2 \cdot CO_2 + 3 \cdot H_2O \quad \Delta H^{BRN}_{298K} = -1279$ kJ/mol

$CH_4 + 2 \cdot O_2 \rightarrow CO_2 + 2 \cdot H_2O \quad \Delta H^{G}_{298K} = -803.1$ kJ/mol

The mass and energy balances for the burner reactor are presented in the Appendix.

## 3. Proton exchange membrane fuel cell

A fuel cell stack is constituted by an anode, where the fuel is injected, and a cathode, where the oxidant, normally oxygen or air, is supplied. The electrodes are separated by a semipermeable membrane that allows the protons exchange and promotes the oxidation reaction to produce electrical power. The cell generates an open-circuit voltage which is affected by a number of losses (activation, concentration and ohmic) that leads to a useful actual voltage. The rigorous dynamic model of a PEM-FC used in this work is taken from [20]. Therefore, only the most important concepts and differential equations are included. In addition, the details about some useful modifications, needed for simulating the complete case, are given. Hence, the PEM-FC was adapted to produce a maximum power of 10 kW. In the book of Pukrushpan firstly considered that the anode is feeded with hydrogen provided by a tank and then he analyzed a complete BPS based on partial oxidation of natural gas.

The PEM-FC considered here converts chemical energy directly into electrical energy, where the overall reaction is

$$H_2 + \frac{1}{2}O_2 \rightarrow H_2O + \text{Heat} + \text{Electrical power}$$

The chemical energy released from the FC can be calculated from the change in Gibbs free energy ($\Delta g_f$) which is the difference between the free energy of the products and the reactants. The Gibbs free energy represents the available energy to do external work, it varies with both, temperature and pressure, and can be calculated as ([28]):

$$\Delta g_f = \Delta g_f^0 - \overline{R} T_{fc} \ln\left[\frac{p_{H_2} p_{O_2}^{\frac{1}{2}}}{p_{H_2O}}\right] \quad (9)$$

where $\Delta g_f^0$ is the Gibbs free energy at standard pressure, $T_{fc}$ is the operating temperature of the FC expressed in Kelvin degrees. The partial pressures, $p_{H_2}$, $p_{O_2}$ and $p_{H_2O}$ of the hydrogen, oxygen, and vapor, respectively, are expressed in Bar. $\overline{R}$ is the universal gas constant 8.31451 J/(kg K). The Gibbs free energy of the reaction is given in [28]. If $\Delta g_f^0$ is negative means that the energy is released from the reaction.

If the fuel cell process could be "completely reversible", the overall Gibbs free energy would be converted to electrical energy, which is the electrical work used to move electrical machine around a circuit. For each mole of hydrogen, 2 mol of electrons pass around the external circuit and the electrical work done (charge × voltage) is equal to $-2FE$ Joules, where

F is the Faraday constant (F = 96485 Coulombs), and E is the voltage of the FC. This electrical work done would be equal to the change in Gibbs free energy if the system is considered ideally reversible ($\Delta g_f = -2FE$). Thus, using eq. (9), the reversible voltage of the FC can be written as

$$E = \frac{-\Delta g_f}{2F} = \frac{-\Delta g_f^0}{2F} + \frac{\overline{R}T_{fc}}{2F}\ln\left[\frac{p_{H_2}p_{O_2}^{\frac{1}{2}}}{p_{H_2O}}\right] \quad (10)$$

However, real fuel cell system is not reversible, so some of the chemical energy is converted to heat, and the FC voltage, $V_{fc}$, is less than in Eq. (10). Voltage E is called the reversible open-circuit voltage or "Nernst" voltage of a hydrogen FC. The term $-\Delta g_f^0/2F$ varies with the temperature from standard state of reference potential (1.229 V) in accordance to:

$$-\frac{\Delta g_f^0}{2F} = 1.229 + (T_{fc} - T_0)\left(\frac{\Delta S^0}{2F}\right), \quad (11)$$

where $T_0$ is the standard state of temperature and $\Delta S^0$ is the entropy variation. Since the entropy change of a given reaction is approximately constant and can be set to the standard value,

$$-\frac{\Delta g_f^0}{2F} = 1.229 - \frac{298.15\cdot\Delta S^0}{2F} + \left(\frac{\Delta S^0}{2F}\right)T_{fc} \quad (12)$$

Using thermodynamic values of the standard state entropy change. Fuel ($H_2$) and oxidant ($O_2$) are considered fully humidified, so their vapor pressure are estimated as at saturated condition. So Eq. (12) is further expanded and yields

$$E = 1.229 - 0.85\times10^{-3}(T_{fc} - 298.15) + 4.3085 \times 10^{-5}T_{fc}\left[\ln\left(p_{H_2}\right) + \frac{1}{2}\ln\left(p_{O_2}\right)\right] \quad (13)$$

In Eq. (13), $T_{fc}$ is expressed in Kelvin degrees, and $p_{H_2}$ and $p_{O_2}$ are expressed in atm. When the FC operates, the actual voltage is less than the calculated value. This discrepancy obeys to the following losses:

$$\text{activation loss}: \quad v_{act} = a\ln\left(\frac{i}{i_0}\right)$$

$$\text{ohmic loss}: \quad v_{ohm} = i\cdot R_{ohm}$$

$$\text{concentration loss}: \quad v_{conc} = i\cdot\left(c_2\frac{i}{i_{max}}\right)^{c_3}$$

where $a$ is a constant, and $i_0$, the exchange current density is constant too. $R_{ohm}$ is the internal electrical resistance with units of $\Omega\ cm^2$. Constants $c_2$,$c_3$ and $i_{max}$ depend on the temperature and the reactant partial pressure, taken from the same reference. The parameters for estimating the voltage losses were obtained adjusting the equations given above to the data of a fuel cell operating at steady state and at specific conditions.

The nonlinear dynamic model developed by [20] is used here but adapted to be proper for the design conditions of the BPS. It is based on electrochemical, thermodynamic and zero-dimensional fluid mechanics principles. Basically, the slower dynamics associated with temperature regulation and heat dissipation are avoided and is focussed in the reactant pressure and flow behavior. Here, it is also assumed the stack average temperature perfectly regulated as well as the inlet reactant flows in the cathode and anode. In addition, it is considered that they are humidified, heated and cooled in a consistent and rapid way. Thus, the dynamic model has a state-space representation with nine sates as can be observed through the Eqs. (14)–(22). The principle of the mass conservation applied in the cathode is given by the Eqs. (14)–(16) for the oxygen, nitrogen and water respectively. Similarly, the governing equations for hydrogen and water in the anode are given by Eqs. (17) And (18). The dynamic of air supercharging device is governed by the compressor inertia in Eq. (19) with $J_{cp} = 5\times10^{-5}\ kg/m^2$. The rate of variation of the mass inside the manifold and the supply manifold pressure are given by the Eqs. (20) And (21) using the principles of mass and energy conservation respectively, where $R_a$ represents the air gas constant. Finally, the return manifold pressure is governed by the mass conservation and the ideal gas law through isothermic assumptions given by Eq. (22).

$$\frac{dm_{O_2}}{dt} = W_{O_2,in} - W_{O_2,out} - W_{O_2,react} \quad (14)$$

$$\frac{dm_{N_2}}{dt} = W_{N_2,in} - W_{N_2,out} \quad (15)$$

$$\frac{dm_{H_2O,ca}}{dt} = W_{H_2O,ca,in} - W_{H_2O,ca,out} + W_{H_2O,gen} + W_{H_2O,mbr} \quad (16)$$

$$\frac{dm_{H_2}}{dt} = W_{H_2,in} - W_{H_2,purge} - W_{H_2,react} \quad (17)$$

$$\frac{dm_{H_2O,an}}{dt} = W_{H_2O,an,in} - W_{H_2O,an,out} + W_{H_2O,mbr} \quad (18)$$

$$J_{cp}\frac{\omega_{cp}}{dt} = \frac{(P_{cm} - P_{cp})}{\omega_{cp}} \quad (19)$$

$$\frac{dm_{sm}}{dt} = W_{cp} - W_{ca,in} \quad (20)$$

$$\frac{dp_{sm}}{dt} = \frac{\gamma R_a(W_{cp}T_{cp,out} - W_{ca,in}T_{sm})}{V_{sm}} \quad (21)$$

$$\frac{dp_{rm}}{dt} = \frac{R_aT_{rm}(W_{ca,out} - W_{rm,out})}{V_{rm}} \quad (22)$$

The compressor air mass flow rate is modeled by the nonlinear curve fitting method and the compressor motor dynamic, resulting a function of the compressor motor input voltage and the supply manifold pressure, $W_{cp} = f(v_{cm},p_{sm})$. The thermodynamic equations are used to calculate the exit air temperature, $T_{cp,out}$ and the required compressor power, $P_{cp}$. The air flow rate in and out of the cathode ($W_{ca,in}$, $W_{ca,out}$) are functions of the difference between the pressure of the gas upstream and downstream, and are approximated by a linear nozzle equation $W = k(p_1 - p_2)$. The flow rates of each element ($O_2$, $N_2$, vapor) are determined using thermodynamic and psychrometric properties of the gas upstream. The return

manifold exit flow rate, $W_{rm,out}$, is calculated using nonlinear nozzle equation for accounting possible large pressure drops. The rates of oxygen and hydrogen reacted and the water generated are function of the stack current (using electrochemical relationships), $W_{O_2,react} = k_o I_{st}$, $W_{H_2,react} = k_h I_{st}$ and $W_{H_2O,gen} = k_{H_2O} I_{st}$ respectively. Where, $k_o$, $k_h$ and $k_{H_2O}$ take into account the number of cells, the Faraday number and the molar mass for each component. Therefore, for determining the hydrogen production setpoint for the BPS a good approximation can be taken through the following relationship:

$$W_{H_2} = \frac{n \cdot I_{st}}{2 \cdot F}, \tag{23}$$

where $W_{H_2}$ refers to $H_2$ production, $n$ is the number of cells in the stack and $F$ the Faraday constant. Even though the hydrogen production should be determined directly from $H_2$ partial pressure in the anode, but this is a variable that cannot be easily measured in an FC. The mass flow of vapor across the membrane, $W_{H_2O,mbr}$, is calculated using mass transport principles and the membrane properties. It is assumed that all the hydrogen is completely utilized by the stack, meaning the purge rate is equal to zero, so the steady-state consumption of fuel constitutes an acceptable approximation for the $H_2$ flow demanded by the stack. To adapt the fuel cell to the power requirements, the number of cells in series is set to $n = 80$ in the PEM-FC model. The new working point needs the optimization of the operation of the FC. There is an optimal oxygen excess, $\lambda_{O_2}^{opt}$, for each demanded current. That condition also determines an optimal voltage to the compressor, net power obtained and pressure of the supply manifold. Using the model and making an analysis as recommended by [29], the new optimal operating conditions can be determined. The net power obtained for different currents, under optimal compressor voltage can be seen in Fig. 2(a). Under the same conditions, the ideal voltage for the compressor can be obtained, as shown in Fig. 2(b). Fig. 2(c) shows the optimal oxygen excess under the new operating conditions. The equations for the approximation to a quadratic function are presented:

$$P_{max}^{net} = -8.57 \times 10^{-2} I_{st}^2 + 60.64\, I_{st} - 223.97 \tag{24}$$

$$v_{CM}^{opt} = 1.19 \times 10^{-3} I_{st}^2 - 9.63 \times 10^{-2}\, I_{st} + 47.29 \tag{25}$$

$$\lambda_{O_2}^{opt} = 5.90 \times 10^{-5} I_{st}^2 - 1.80 \times 10^{-2} I_{st} + 4.78 \tag{26}$$

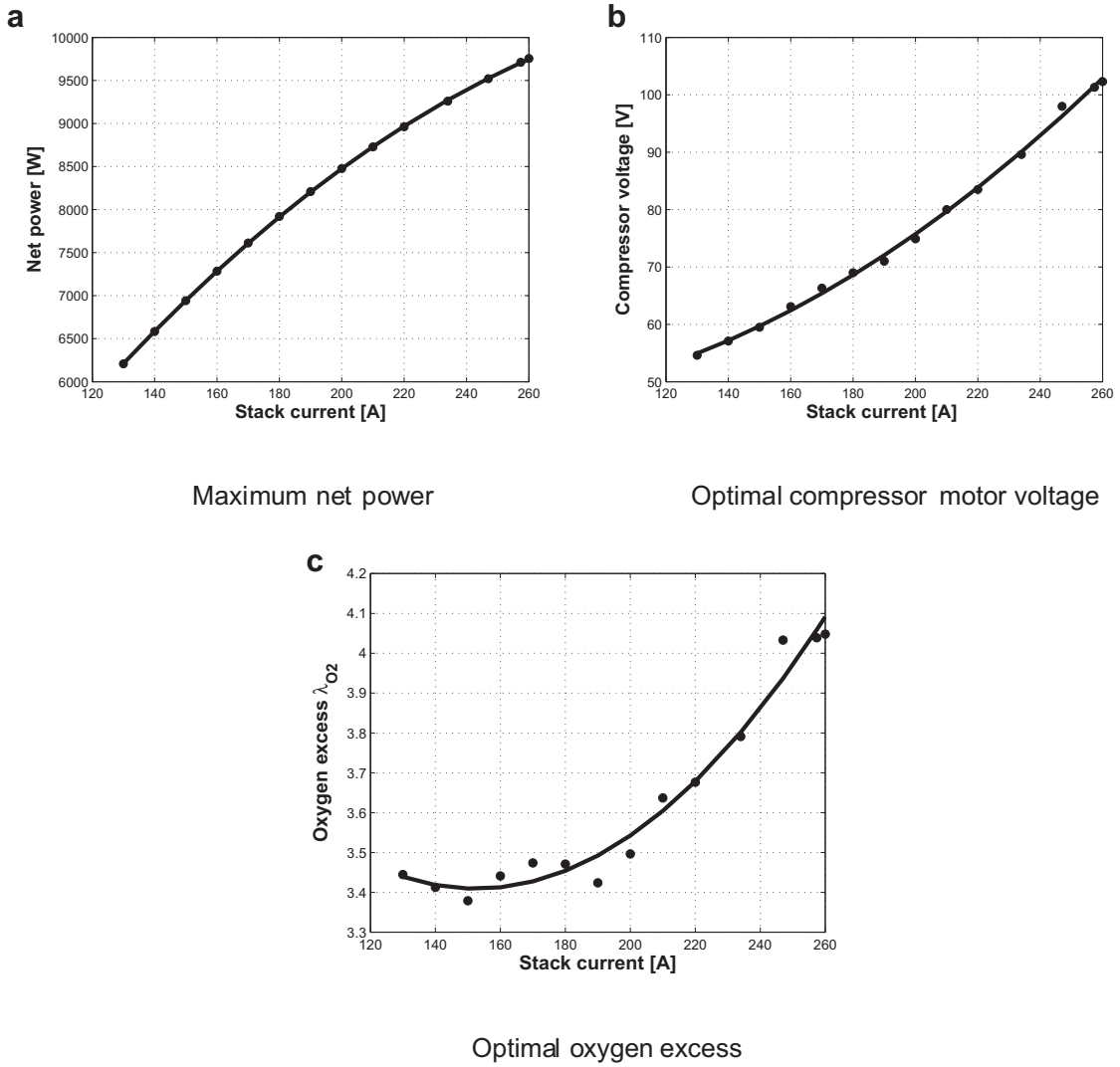


**Fig. 2 – Optimal values for different current loads.**

The net power grows inside the interval considered here with such concavity which leads to assume that an upper bound is present. The compressor motor voltage needed for this system presents a different concavity since it grows quadratically. On the other hand, the behavior of the oxygen excess is radically different. It has a minimum in the interval. Hence, it is not possible considering a fixed setpoint for this variable. It must be approximated by the quadratic function obtained here.

## 4. Computational implementation of the mathematical model

The computational implementation of the mathematical model takes into account the specific tools that each commercial software is able to offer. The auxiliary equipments for satisfying the pressure requirements such as compressors and turbines as well as the burner CSTR are modeled in HYSYS® environment. In addition, it supports the important data bank about properties information for the different components that are part of the process. The heat exchangers network is simulated by 'LNG' tool, which will be well detailed in the next section. All the parts described above run in steady state and are called by MATLAB® each integration interval. The reason of splitting the plant between both programs lies on the dynamic characteristics of the different parts of the process. In HYSYS are the equipments with faster responses, the other reason is related to take advantage of the useful tools available in HYSYS. The rest of the plant is dynamically modeled in MATLAB®, such as the plug flow reactors and the PEM-FC. The differential equations corresponding to their mathematical model are integrated in MATLAB where an important part of the data is obtained from HYSYS®.

In order to successfully coordinate calculations between these programs, an Activex-com controller for HYSYS® is needed, which is in a directory named ***hysyslib*** that should be installed in the toolboxes and addressed to the MATLAB® path. This interface is sustained by the use of the spreadsheets of HYSYS® for the transference and actualization of the information. The spreadsheet is a grid that contains all the values of the variables needed for the interchange in specific cells that are easily identified. Hence, MATLAB® is able to connect to these specific grids, read and write all the data that is available every integration interval.

### 4.1. *Heat integration*

For constructing the pseudo dynamic model it was taken into account that heat exchangers have fast responses compared to other unit operations in a process. Normally the time constant is measured in seconds but could be up to a few minutes for larger equipments. The heat exchangers should be modeled rigorously by partial differential equations since they are distributed systems. This introduces the correct amount of dead time and time constant in the exit stream temperatures, but the models are difficult to solve. It was found that for the purpose of plant-wide control studies it is not necessary to have such detailed descriptions of the exchanger dynamics, since these units rarely dominate the process response. Luyben et al. [30] considered that another alternative is to use an effective method to calculate the steady-state exchanger exit temperatures and then delay these temperatures by first order time constants to capture the dynamics. Even though the LNG tool of HYSYS® works only in steady state mode, it allows doing the simulation of the heat exchangers network based on the considerations given above about their fast responses. This methodology does not need knowing all the details of the network configuration. The minimum heat requirement of the system and the minimum heat to be evacuated can be computed for each operating point or with the system under different disturbances. It is done by solving material and heat balances for multi-stream exchangers. Each stream is divided in a number of intervals, in this case, ten intervals are considered. The LNG unit allows analyzing the system energy integration by means of the Pinch technology, as described in [31]. For beginning with the process integration study a list of hot and cold streams, which define heat sources and heat requirements of the system must be performed. The heat exchange is technically feasible only if the difference between the temperatures of the hot and cold streams is always superior to a predefined $\Delta T_{min}$, and the maximum heat recovery is obtained when the $\Delta T_{min}$ constraint is activated. This point is called the Pinch point.

## 5. Linear model development

The mathematical developing of the rigorous pseudo dynamic model presents nonlinear differential equations. A common practice is to convert it into a reduced order model with linear differential equations. This approach allows the use of the powerful linear mathematical techniques and is helpful for doing preliminary tests with less computational time. However, the linearization must be done around a steady state point. Here, the chosen steady state operating point is related to that able to achieve the maximum efficiency. Therefore, the first requirement is selecting a minimum number of variables that have to be controlled to guarantee that the process is stabilized at the specified operating point. In this case, a typical selection is the pressure of each reactor (ESR, HTS, LTS, CO-PrOx) as the primary control loops needed to stabilize the process. They are configurated by manipulating their corresponding exit flows. Another important variable here is the hydrogen production rate which is controlled by manipulating the fresh ethanol inlet flow. The pressure loops are assumed under perfect control and they are identified in the Table 1 with (*), and the production loop with (**). Then, the linearized model is obtained here by applying a system identification technique. It is very useful for obtaining a preliminary plant-wide control design and tuning with less computational effort than using the rigorous nonlinear model. In Table 1 are listed fourteen outputs ($y_1$–$y_{14}$), six potential manipulated inputs ($u_1$–$u_6$) and two disturbances ($d_1$ and $d_2$). All of them are available for identification purposes. Then, the inputs of the process must be excited with rich signals and collect the output data periodically with a suitable sample time, $T_s$. The input signals are selected as random steps whose amplitudes vary between ±5% (wide-range of linearization) from their nominal values.

**Table 1 – Variables in the BPS + FC process.**

| Measured | | Manipulated | | Disturbances | |
|---|---|---|---|---|---|
| $y_1$ | ESR exit temperature | $u_1$ | Water to ESR inlet | $d_1$ | Ethanol purity |
| $y_2$ | Jacket exit gases temperature | $u_2$ | Exchanged heat Q | $d_2$ | Stack current |
| $y_3$ | Burner exit temperature | $u_3$ | Ethanol to Burner | | |
| $y_4$ | Burner entering molar flow | $u_4$ | Oxygen to Burner | | |
| $y_5$ | Molar ratio $H_2O$/Ethanol | $u_5$ | Oxygen to CO-PrOx | | |
| $y_6$ | HTS exit temperature | $u_6$ | CM voltage | | |
| $y_7$ | LTS exit temperature | $u_7$ | ESR exit flow(*) | | |
| $y_8$ | CO-PrOx exit temperature | $u_8$ | HTS exit flow(*) | | |
| $y_9$ | Molar ratio $O_2$/CO | $u_9$ | LTS exit flow(*) | | |
| $y_{10}$ | Burner exit molar flow | $u_{10}$ | CO-PrOx exit flow(*) | | |
| $y_{11}$ | CO-PrOx CO exit concentration | $u_{11}$ | Bio-ethanol flow(**) | | |
| $y_{12}$ | Net Power | | | | |
| $y_{13}$ | Oxygen excess | | | | |
| $y_{14}$ | Stack voltage | | | | |
| $y_{15}$ | ESR pressure(*) | | | | |
| $y_{16}$ | HTS pressure(*) | | | | |
| $y_{17}$ | LTS pressure (*) | | | | |
| $y_{18}$ | CO-PrOx pressure (*) | | | | |
| $y_{19}$ | $H_2$ production rate (*) | | | | |

The time needed for achieve the steady state of the plant is about of 5 s. Then, adopting a sample time of $T_s = 0.05$ s, allows to collect about 100 samples per step change. The recorded data base is pre-processed by normalization to zero mean and unit variance for all variables before starting the identification procedure.

Basically, all the subspace state-space System Identification methods are based on system theory, numerical linear algebra and projections tools. A classical algorithm is the well-tested "n4sid" method developed by [32] and implemented in Matlab® by [33,34]. This strategy allows to estimate the system matrices of the state-space linear model, $\hat{\mathbf{A}}$, $\hat{\mathbf{B}}$, $\hat{\mathbf{C}}$, $\hat{\mathbf{D}}$ and the model order using singular value decomposition from the impulse response Hankel matrix. It is obtained from the data by solving a linear least squares problem.

Hence, in Eq. (27) is represented the linear state-space model structure and in Eq. (28) the corresponding matrices dimensions are included for representing the BPS with PEM-FC dynamic behavior.

$$\begin{aligned}\mathbf{x}(k+1) &= \hat{\mathbf{A}}\mathbf{x}(k) + \hat{\mathbf{B}}\mathbf{u}_t(k)\\ \mathbf{y}(k) &= \hat{\mathbf{C}}\mathbf{x}(k) + \hat{\mathbf{D}}\mathbf{u}_t(k)\end{aligned} \tag{27}$$

where $\mathbf{u}_t(k) = [\mathbf{u}, \mathbf{d}]^T$ is the model input vector containing the manipulated input vector $\mathbf{u} = [u_1, u_2, u_3, u_4, u_5, u_6]^T$ and the disturbance vector $\mathbf{d} = [d_1, d_2]^T$. With

$$\hat{\mathbf{A}} : [15 \times 15];\ \hat{\mathbf{B}} : [15 \times 8];\ \hat{\mathbf{C}} : [14 \times 15];\ \hat{\mathbf{D}} : [14 \times 8] \tag{28}$$

where $\mathbf{x}$ is the state vector of dimension [15 × 1], $\mathbf{y}$ is the output vector of dimension [14 × 1] and $\mathbf{u}_t$ is the input vector of dimension [8 × 1]. The elements of each matrix ($\hat{\mathbf{A}}$, $\hat{\mathbf{B}}$, $\hat{\mathbf{C}}$ and $\hat{\mathbf{D}}$) are included in the Appendix.

The data base obtained from the experiments was divided in two groups. One called *estimation data* to develop the discrete state-space linear model shown in Eq. (27), and the second one called *validation data* to test the accuracy of the model predictions. The order of the model was chosen according to a trade-off between the model size (amount of states) and the mean square prediction error.

A very good approximation (either for steady states and transients) is achieved with the obtained reduced order model. Then, it will be helpful for obtaining a preliminary control structure and to tune the controllers. Another useful information is the steady state gains of the model. Since the state-space model given in Eq. (27) is linear, a discrete transfer function of the system can be obtained by

$$\mathbf{G}(z) = \hat{\mathbf{C}}(zI - \hat{\mathbf{A}})^{-1}\hat{\mathbf{B}} + \hat{\mathbf{D}} \tag{29}$$

Applying the final value theorem the steady state magnitudes can be obtained by:

$$\lim_{t\to\infty}[\mathbf{Y}(t)] = \lim_{z\to 1}\left[(1 - z^{-1})\mathbf{Y}(z)\right] \tag{30}$$

$$\mathbf{Y}(z) = \sum_{k=0}^{\inf}\mathbf{y}(k)z^{-k} \tag{31}$$

They can be seen in Table 2, normalized for the manipulated variables, and two disturbances, with the identified outputs. Matrices $\mathbf{G}$ and $\mathbf{D}$ from the Table 2 refer to the steady state gains of the model, corresponding to the Equation (32) :

$$\mathbf{Y} = \mathbf{G}\mathbf{u} + \mathbf{D}\mathbf{d} \tag{32}$$

Where $\mathbf{Y}$ is the normalized steady state output vector of dimension [14 × 1]. Matrices $\mathbf{G}$ and $\mathbf{D}$ are defined as

$$\mathbf{G} = \begin{bmatrix} k_{p1,1} & \cdots & k_{p1,6} \\ k_{p2,1} & \cdots & k_{p2,6} \\ \bullet & \cdots & \bullet \\ k_{p14,1} & \cdots & k_{p14,6} \end{bmatrix};\ \mathbf{D} = \begin{bmatrix} k_{d1,1} & k_{d1,2} \\ k_{d2,1} & k_{d2,2} \\ \bullet & \bullet \\ k_{d14,1} & k_{d14,2} \end{bmatrix} \tag{33}$$

where $k_{pl,m}$ and $k_{dl,n}$ are the particular steady state gains of the process, with output $l$, input $m$ and disturbance $d$ for manipulated variables and disturbances respectively. They are defined as:

$$k_{pl,m} = \frac{y_{f,l} - y_{ss,l}}{u_{f,m} - u_{ss,m}};\ k_{dl,n} = \frac{y_{f,l} - y_{ss,l}}{d_{f,n} - d_{ss,n}} \tag{34}$$

where $y_f$ is obtained from the final value theorem application shown in Eq. (30) and $y_{ss}$ is the measured variable at the

**Table 2 – Normalized steady-state gains for BPS + FC process.**

| | G | | | | | | D | |
|---|---|---|---|---|---|---|---|---|
| | $u_1$ | $u_2$ | $u_3$ | $u_4$ | $u_5$ | $u_6$ | $d_1$ | $d_2$ |
| $y_1$ | −0.0012 | 0.9250 | 0.0157 | 0.1658 | 0.0030 | −0.0189 | −0.0021 | −0.2811 |
| $y_2$ | 0.1397 | −0.5491 | 0.0615 | 0.6641 | −0.0040 | −0.0015 | −0.0036 | −0.7037 |
| $y_3$ | −0.2998 | −0.2600 | 0.5627 | −0.6554 | 0.0071 | −0.0046 | 0.3538 | 0.4096 |
| $y_4$ | 0.5028 | −0.0852 | 0.0020 | −0.0167 | 0.0541 | −0.0060 | −0.0724 | 0.7594 |
| $y_5$ | 0.6500 | 0.1728 | 0.0080 | 0.0236 | −0.0058 | −0.0040 | 0.2533 | −0.7062 |
| $y_6$ | −0.6530 | 0.6671 | 0.0046 | 0.1194 | −0.0009 | 0.0087 | 0.0966 | −0.1923 |
| $y_7$ | −0.7799 | 0.0793 | 0.0004 | 0.0169 | 0.0056 | 0.0070 | 0.1078 | 0.8877 |
| $y_8$ | −0.9448 | −0.0536 | −0.1032 | 0.1095 | 0.3593 | 0.1900 | 0.3286 | −0.0847 |
| $y_9$ | 0.7183 | 0.0184 | 0.0024 | −0.0139 | 0.1876 | −0.0125 | −0.1250 | −0.9165 |
| $y_{10}$ | 0.2080 | −0.0347 | 0.0888 | 0.9650 | 0.0023 | −0.0013 | −0.0048 | 0.0400 |
| $y_{11}$ | −0.2903 | 0.1212 | 0.0856 | −0.0709 | −0.0680 | −0.1415 | −0.1304 | 0.6714 |
| $y_{12}$ | 0.0115 | 0.0167 | 0.0045 | −0.0018 | 0.0066 | −0.0609 | 0.0087 | 0.8192 |
| $y_{13}$ | −0.0027 | 0.0005 | 0.0001 | 0.0013 | 0.0020 | 0.7526 | −0.0010 | −0.5717 |
| $y_{14}$ | 0.0017 | 0.0062 | 0.0017 | −0.0026 | 0.0003 | 0.4741 | 0.0031 | −0.8188 |

wanted operating point. $u_f$ and $u_{ss}$ are final and nominal condition for the manipulated and $d_f$ and $d_{ss}$ the same for disturbances. All of this information facilitates the preliminary control analisys. Then, the final tests are done on the rigorous nonlinear pseudo dynamic model to define the final plant-wide control structure and tuning.

## 6. Control structure

The main objectives of the BPS control are to maintain $H_2$ levels on the anode of the FC, because starvation can cause permanent damage, and overfeeding will lead to $H_2$ waste. In addition, the CO levels of the anode inlet stream must be under 10 parts per million (volume), and the temperatures of the reactors set and FC must be inside specific range to prevent damages, maintaining the overall system efficiency.

In [21] a preliminary control structure was proposed, based on a disturbances sensitivity analisys, as was proposed by [30], performed with only steady state information. In that work the control loops were determined for rejecting two critical disturbances. A more deep studio is presented here where other important process objectives are taken into account. Hence, the total control loops considered here are schematically shown in Fig. 3 and detailed in Table 3. The most critical controlled variables were selected taking into account the objectives mentioned above, directly related to the optimal operating conditions of the BPS and PEM-FC. Hence, in this work, the control structure is mainly determined based on the process knowledge.

Another important issue to be solved is to have a methodology for obtaining acceptable tuning parameters for the multivariable controller. In this stage the linearized model around the optimal operating point can be adopted as a nominal model for implementing a tuning strategy based on internal model control (IMC) theory. This method was selected because it has proven good performance in control schemes for chemical plants. The tuning parameters were chosen following the recommendations given in [35], and they are shown in Table 4.

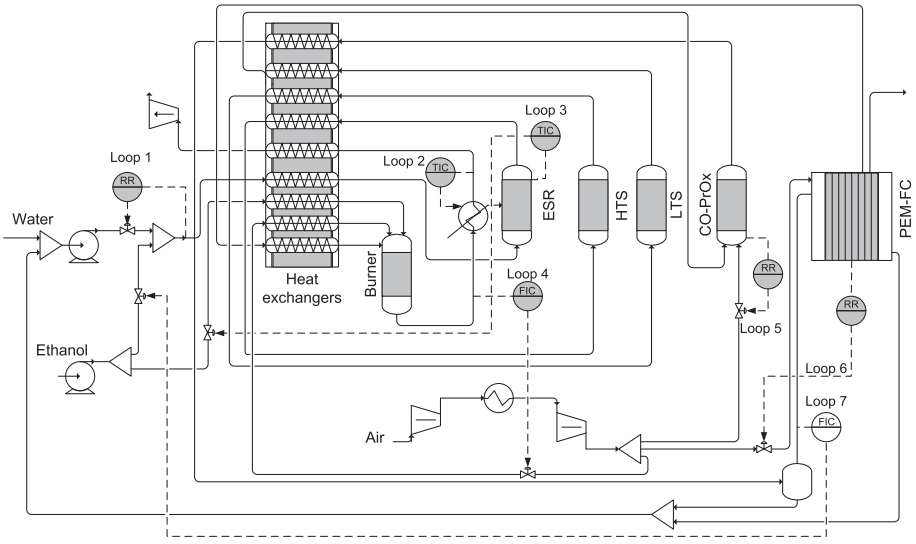


**Fig. 3 – Implemented control structure.**

**Table 3 – Detail of the control loops.**

| | Controlled | Manipulated |
|---|---|---|
| loop 1 | $y_5$ | $u_1$ |
| loop 2 | $y_1$ | $u_2$ |
| loop 3 | $y_3$ | $u_3$ |
| loop 4 | $y_{10}$ | $u_4$ |
| loop 5 | $y_9$ | $u_5$ |
| loop 6 | $y_{13}$ | $u_6$ |
| loop 7 (**) | $y_{19}$ | $u_{11}$ |

**Table 4 – Controllers tuning.**

| | loop 1 | loop 2 | loop 3 | loop 4 | loop 5 | loop 6 | loop 7 (**) |
|---|---|---|---|---|---|---|---|
| $k_c$ | 0.005 | 0.039 | $4.5 \times 10^{-5}$ | 0.001 | $1 \times 10^{-6}$ | 5.071 | 100 |
| $\tau_i^c$ | 2.671 | 3.327 | 0.055 | 0.047 | 0.05 | 0.140 | 0.1 |

## 7. Simulation results with the dynamic model

The simulation results are divided in three main parts according to the different steps followed during the model development. They consider the model validation, the details of the obtained state-space linearized model and the tests of the control structure design implemented here.

### 7.1. *Reactors profiles and validation of the model*

The pseudo dynamic model is able to show several interesting information about the obtained profiles of the reforming reactor for composition and temperatures in the jacket and inside the unit as can be seen at Fig. 4. It can be noticed that the consumption of ethanol has an important increase in the entrance of the reactor, producing a maximum in the acetaldehyde concentration. At the same position the temperature inside the reactive bed decreases. After the acetaldehyde reaches its peak, it decreases gradually to almost disappear at the exit of the reactor. The slow diminution of the amount of water inside the reactor is directly related with the increase in hydrogen concentration. Methane also presents a maximum, and then decreases up to lowest value at the end of the reactor. Carbon oxides present a sudden increase in the concentration and then keep nearly constant along the rest of the reactor. According to the endothermic reaction of the reformer, the temperature profiles show in the first section a relatively abrupt decrease of the temperature in the hot gases inside the jacket and then continue decreasing gradually. This behavior is explained because they transfer the necessary energy to produce the reforming reaction. The range of the internal temperature of the reactor is adequate to allow an acceptable hydrogen production.

For the steady state operation, the substances present an evolution through the length of the processor. In Fig. 5 the composition profile for the hydrogen is shown along the reactors. The curves are proportional to the position inside each reactor. The concentration begins in zero value, meaning that there is no $H_2$ in the inlet flow. The first reactor, the ESR produces most of the hydrogen, as stated previously. The second reactor, the HTS, produces more hydrogen, and the third, the LTS, produces even more, reaching equilibrium at the end of its length. Finally, the CO-PrOx reactor consumes a small amount of hydrogen in an undesired combustion. The concentration suffers a decreasing step at the inlet of this last reactor, because of the amount of air injected, it reduces the concentration abruptly by the increase of flow, but does not affect the amount of hydrogen in the stream.

Another important reactant is the carbon monoxide. The concentration profile can be seen in Fig. 6. This substance is important because it is hazardous and it is necessary to keep in low concentrations. As in the hydrogen case, the inlet stream is free of CO, so it starts in zero value. Some CO appears in the ESR as an intermediate, as commented earlier. In the HTS begins the elimination of this substance, reaching

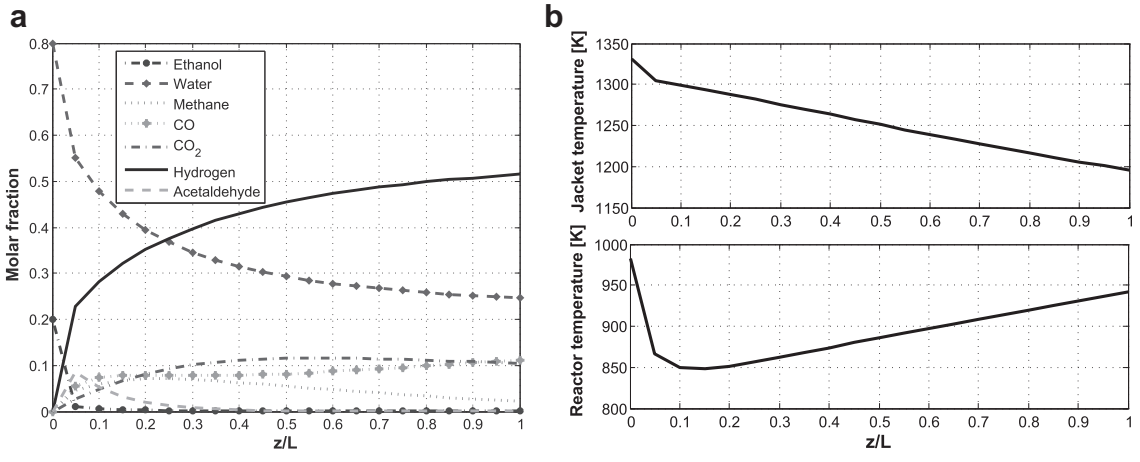


ESR molar composition profile Temperatures profile for ESR

**Fig. 4 – Steady state compositions and temperature profiles for the ESR.**

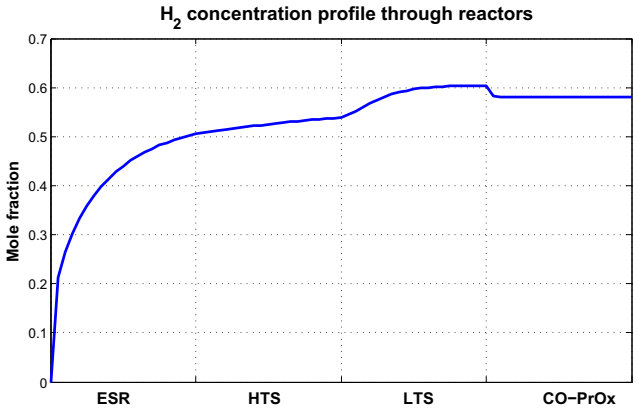


**Fig. 5 – $H_2$ concentration profile.**

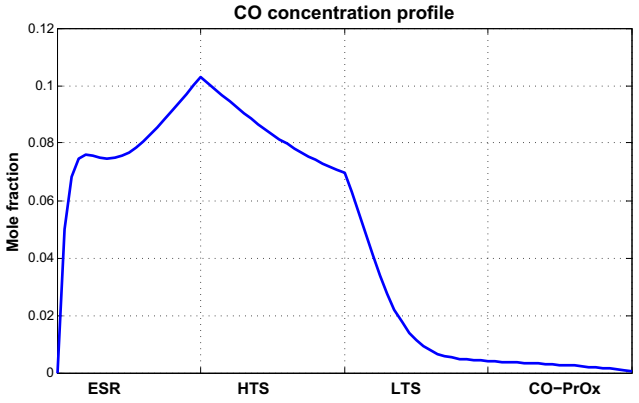


**Fig. 6 – CO concentration profile.**

an equilibrium value in the LTS. The final elimination is done in the CO-PrOx, reaching the concentration values to obtain PEM quality hydrogen rich synthesis gas, to avoid catalyst poisoning.

Finally, in Fig. 7 the temperature profile for the chain of reactors is presented. The first part was analyzed earlier, the corresponding with the ESR reactor, the temperature first decreases, and then rises again to reach nearly the inlet value.

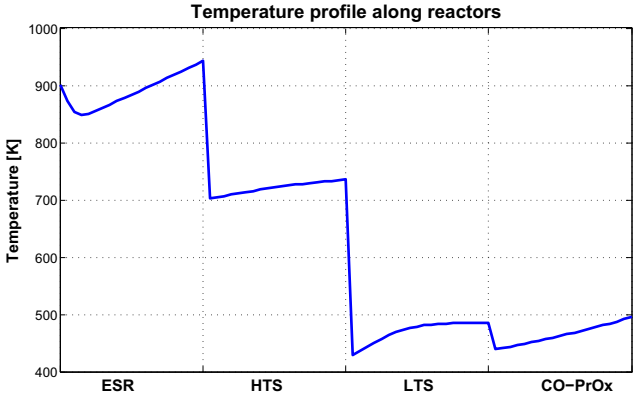


**Fig. 7 – Temperature profile.**

There is a leap between the exit of the ESR and the inlet of the HTS, where the heat exchangers produces the cooling of the stream. Inside the high temperature shift, there is an increase in the temperature, because the WGS reaction is exothermic, and the reactor considered adiabatic. After the second reactor and before the LTS there is another temperature reconditioning. In the LTS, the temperature increases again to reach an equilibrium value. There is a small temperature change at the inlet of the CO-PrOx, and then increases inside that reactor because the combustion reactions are highly exothermic.

### 7.2. *Dynamic linearized reduced model obtention from the rigorous model*

According to the procedure described in sect. 5, the identification experiment is done. The inputs are excited periodically with random steps, and the results recorded to apply a system identification technique. In Fig. 8 the excited variables for the validation data are shown. The first three rows correspond to the 6 manipulated variables considered. They vary around the operating point with a wide range. The two bottom figures represent the considered disturbances, the ethanol purity and the current demanded to the fuel cell stack. This data was preprocessed and normalized to zero mean before applying the SI technique.

The obtained results with the rigorous model, together with the results for the linearized model, can be seen in Fig. 9. The six figures shown correspond with the selected variables to be controlled. These figures are the result of the application of the excited variables shown in Fig. 8. A very good approximation can be obtained with the reduced order model. A complete detail of the overall elements of each matrix of the state-space model is presented in the Appendix. Either for steady state and transients the behavior of both models is remarkably similar, and a small deviation can be assumed when using the linearized model for analysis purposes.

### 7.3. *Closed loop performance*

The pseudo dynamic model presented here is based on the plant-wide synthesis given in [23], which was the first one on doing a deep analysis about the operational conditions for the complete process. The energy balance taking into account the overall plant and the PEM fuel cell for generating electric power gave an optimal operating point for maximum efficiency. Then, it was considered that having a control-oriented model at this point would be useful for obtaining a preliminary plant-wide control structure able to keep the plant very close to it. In addition, an iterative methodology between synthesis and control could be done before the process be constructed. In [30] is recommended to check controllability issues during the plant synthesis stage to evaluate if it is necessary to redesign the process. This represents a valuable mechanism for developing an efficient and well controlled hydrogen production via bio-ethanol to respond to PEM requirements for using in vehicles. The resulting responses were compared to the stationary states reported on [23] for the 10 kW FC. A good agreement with those points were found.

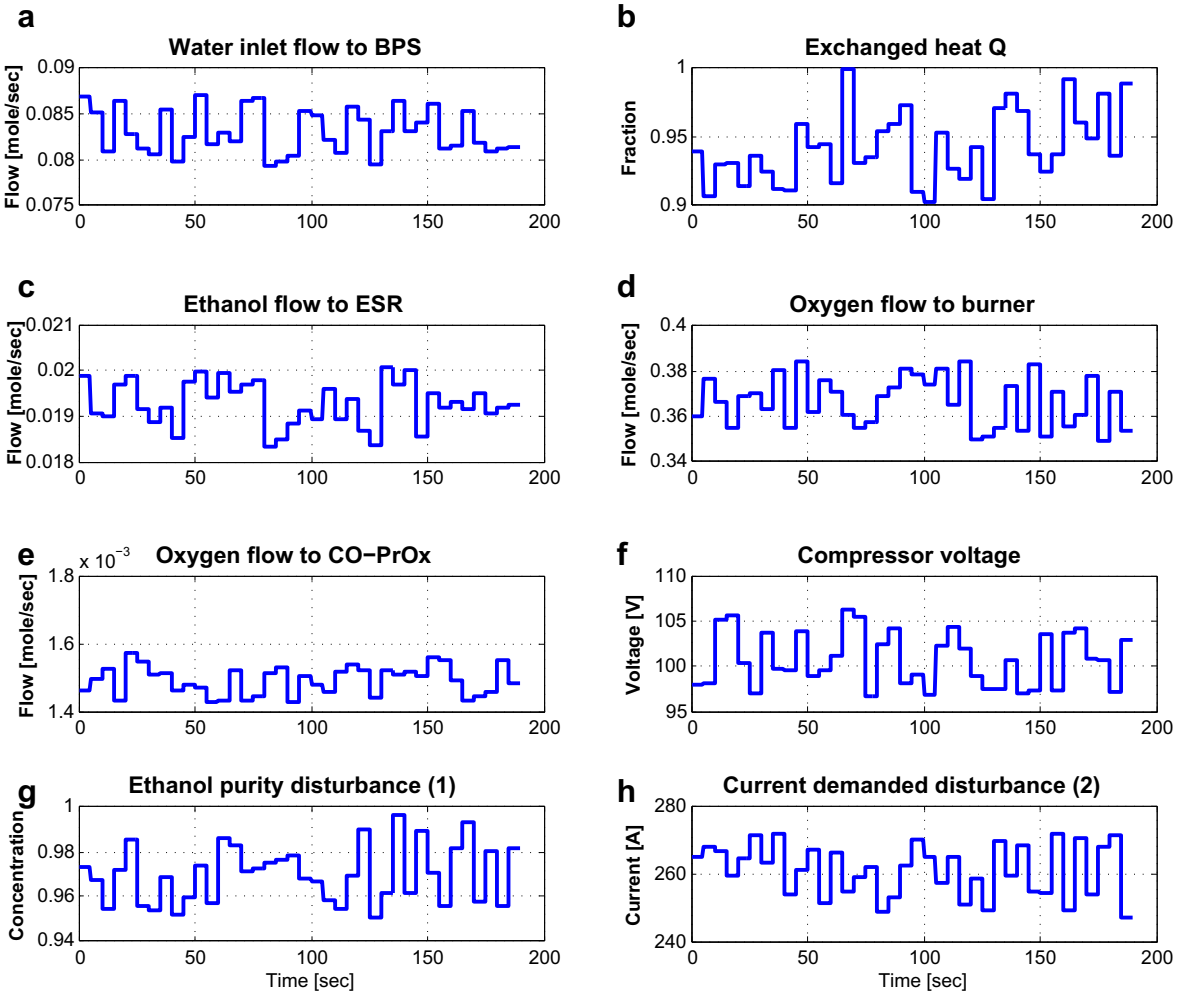


**Fig. 8 – Manipulated variables and disturbances for the validation data.**

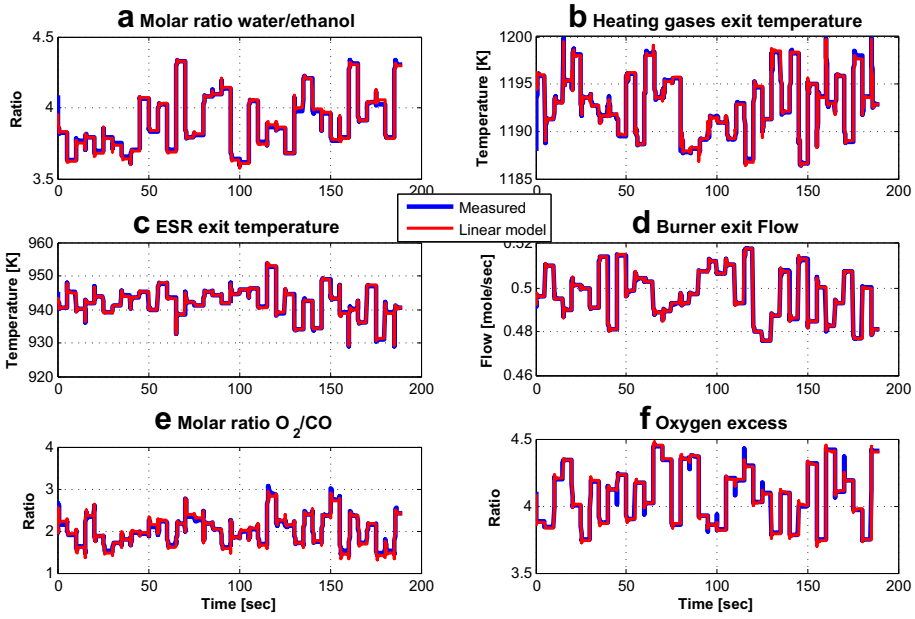


**Fig. 9 – Candidate controlled variables and validation of the linearized model.**

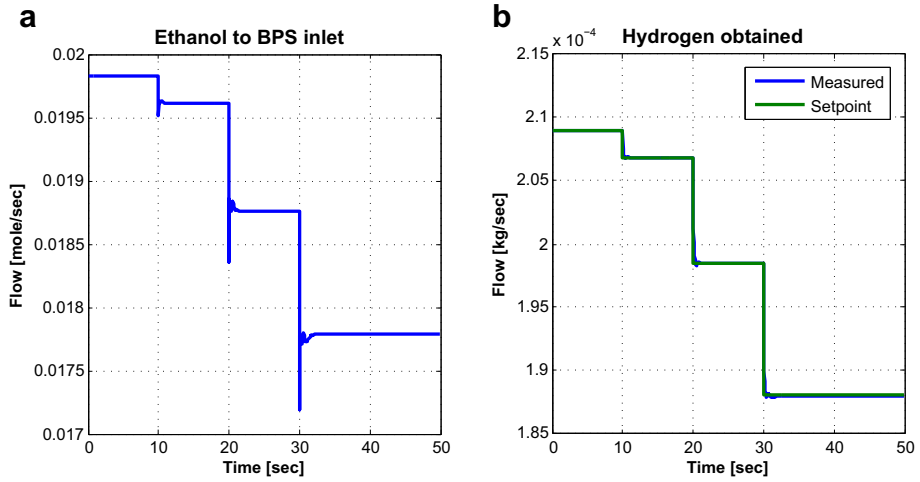


**Fig. 10 – $H_2$ production control loop for current demand change.**

Then, the same step changes considered at [21] were performed here. In Fig. 10 can be seen the dynamic responses when the current is excited by steps of −1%, −5% and −10% at 10, 20 and 30 s, respectively. Fig. 10 presents at the left the manipulated variable, bio-ethanol fresh feed to the BPS, and at the right, the production of hydrogen, the controlled variable. The current demands to the PEM, considered as disturbance, commands the setpoint variations for hydrogen production according to the relationship given in Eq. (23). It can be seen that the hydrogen production responds quickly to these demands which is very important for the electrochemical energy generation. The hydrogen production is kept very close to the imposed setpoint and the ethanol flow to the ESR change rapidly to reject this disturbance effect.

In Fig. 11 the molar ratio water/ethanol at the inlet of the ESR is shown, with the manipulated corresponding variable, the water at the inlet of the processor. The setpoint of the ratio is fixed in 4, and the control loop is able to cope with it quickly and smooth, with small peaks (≈5% in the worst case) of overvalues. The Fig. 12 presents the $O_2$/CO molar ratio at the inlet of the CO-PrOx, together with the oxygen molar flow. Again, the disturbances are properly rejected and the CV kept closely to the setpoint, with small variations but quickly restored. The Fig. 13 presents the only loop considered in the fuel cell, where the compressor motor voltage manipulates the oxygen excess ratio at the outlet of the cathode. As in the $H_2$ production loop, the disturbance considered (the current demanded) influences the optimal oxygen excess and commands the setpoint variation according to the relation given in Eq. (26). The disturbance is properly rejected, and the reference tracking satisfactory. The other variables, which are not shown, presented excellent performance, for both temperatures and flows control.

For the second disturbance, the change in ethanol molar fraction, the variable is excited by steps of −1%, −5% and −10% at 10, 20 and 30 s, respectively. The Fig. 14 presents the resulting hydrogen produced against this abnormal situation. The left graphic shows the manipulated variable, the

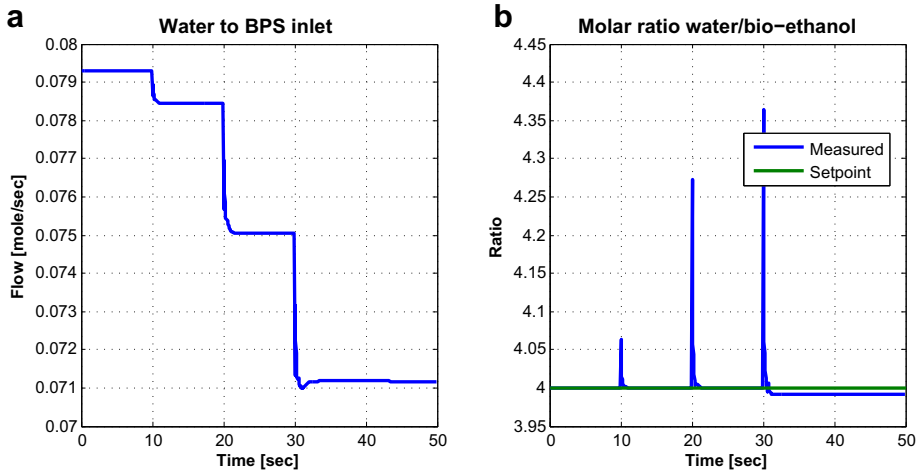


**Fig. 11 – Water feed and water/ethanol ratio at the BPS inlet for current disturbance.**

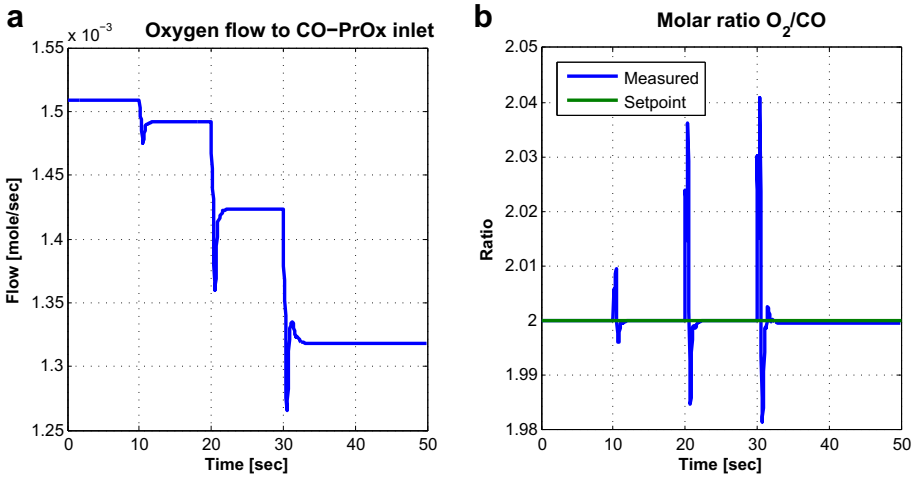


**Fig. 12 – Oxygen inlet and $O_2$/CO ratio at the CO-PrOx reactor under different current demands.**

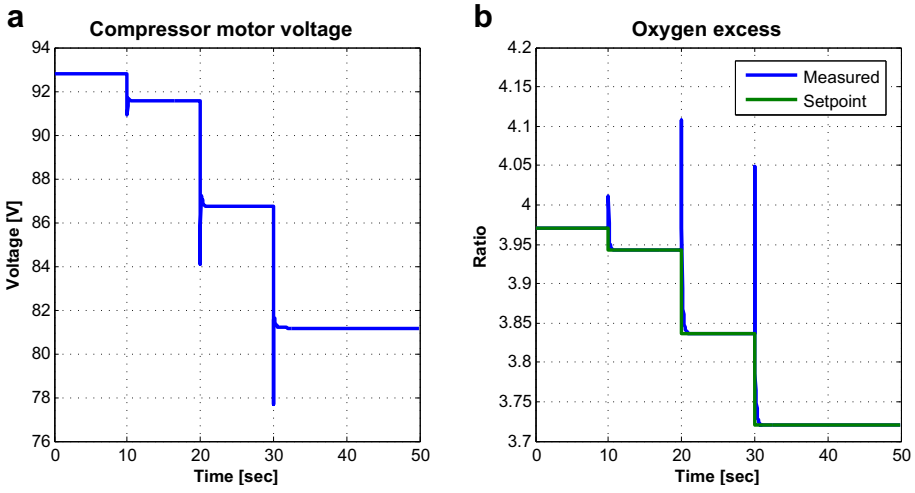


**Fig. 13 – CM voltage and oxygen excess for the fuel cell for changing current demands.**

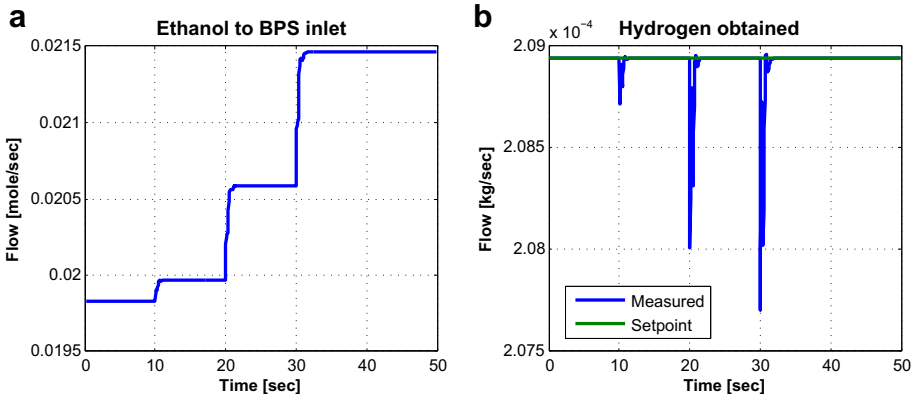


**Fig. 14 – $H_2$ production control loop for ethanol purity disturbance.**

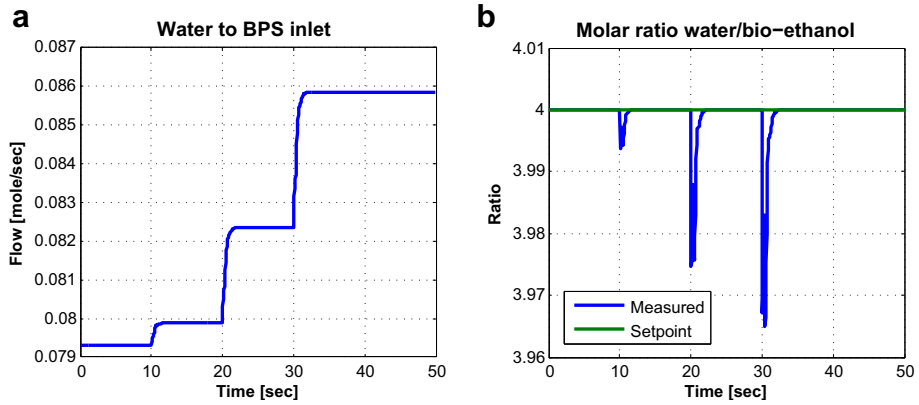


**Fig. 15 – Water feed and water/ethanol ratio at the BPS inlet for ethanol purity change.**

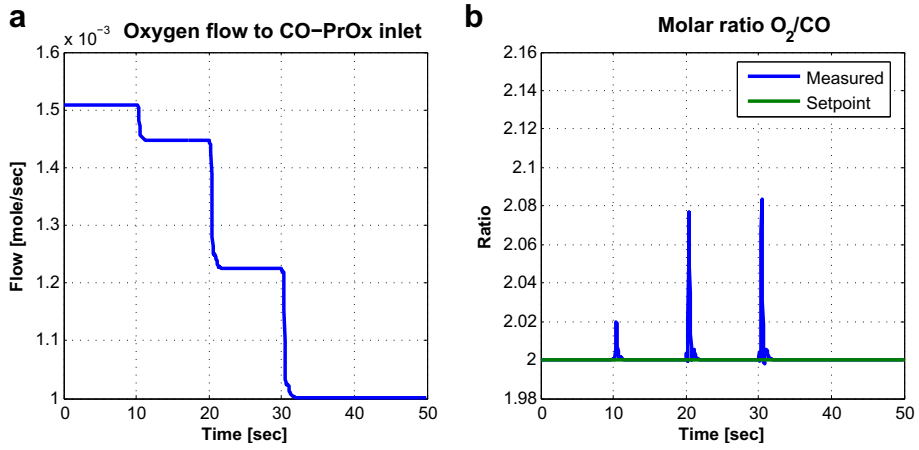


**Fig. 16 – Oxygen inlet and $O_2$/CO ratio at the CO-PrOx reactor for ethanol impurities.**

bio-ethanol fresh feed. The production of hydrogen is quickly restored to its fixed setpoint, with small peaks of under-production, with a smooth change in the feed flow. The behavior of the loop is satisfactory. In Fig. 15 the molar ratio of water/ethanol at the inlet of the BPS is shown, with its corresponding manipulated variable, the water feed. The disturbance rejection is very good. Finally, the Fig. 16 shows the molar ratio of $O_2$/CO at the inlet of the CO-PrOx, showing good performance with small variations around the set-point. The fuel cell stack is not affected by this disturbance. The rest of the controlled variables, corresponding to temperatures and flows, presented very good disturbance rejection.

## 8. Conclusion

In this work, the main characteristics of the rigorous pseudo dynamic model implementation of a Bio-ethanol Processor System along with a Fuel Cell Stack, was presented. This process needs to be highly integrated to obtain good efficiencies and maximum heat recovery. It was necessary to do a deep review about the state of the art concerning this kind of system which currently are at prototype scale. Several researchers are working on topics such as catalysts, kinetics, membranes for the PEM, etc. which still represent open paradigms. Therefore, this model was developed according to the current available information but having in mind that it is an incipient area and new data appears dairy in the literature. Hence, the model is developed enough flexible to analyze other possible kinetics, sizing, etc. and accounting different scenarios for load requirements. In addition, the computational implementation required to properly connect two commercial softwares such as MATLAB and HYSYS accounting their potentiality for simulate this complex process. The model validation was done with only steady state information from a previous work. Some other qualitative aspects could be evaluated through its analogy with other fuel processor system but using different raw material. In this context, currently it was not possible to find exactly the same system data to be confronted with the results obtained here. Hence, it is considered that this is the main contribution of this work. The model works well in the point of maximum efficiency, however, to achieve a successful operation when the typical disturbances occur is necessary to

account with a well designed plant-wide control structure. Looking forward this objective the rigorous pseudo dynamic model allowed obtaining a linearized and reduced order of a dynamic model via system identification techniques. In this context, it was possible to design and test a preliminary control policy based on the knowledge of the plant and its main objectives. The simulation results for both, open and closed loop behaviors, seem to indicate good performances. The composition and temperature profiles for the ESR, the most important reactor of the process and the temperature dynamic behaviors show a qualitative good result. The preliminary tuning parameters for the proposed seven control loops gave quick and smooth responses which represent a good starting point. As future works are considered the use of this pseudo dynamic model to be extended to be completely dynamic. Testing new methodologies of plant-wide control structure and optimal sensor location developed in a systematic way and using as less as possible heuristic concepts. Accounting standard driving cycles profiles, providing from realistic vehicle requirements, to check the complete control structure under these complex scenarios.

## Acknowledgment

The authors thank the financial support of CONICET (Consejo Nacional de Investigaciones Científicas y Técnicas) and ANPCYT (Agencia Nacional de Promoción Científica y Técnica) from Argentina. The authors also acknowledge the support of the UTN-FRRo.

## Appendix.

### *Detailed models for simulation*

*Bio-ethanol steam reformer*

The total mass balance for the ESR is:

$$\frac{dn_{t,k}}{dt} = Fr_{k-1} - Fr_k + [(-r_{A,k}) + (-r_{B,k}) + 2\cdot(-r_{C,k})]\cdot w_{cat} = 0, \quad (35)$$

$k$ stands for the specific slice where the mass balance is performed. Analogously, $(-r_{x,k})$ is the reaction rate for the reaction X, corresponding to reactions A, B, C and D, for each slice.

And the component mass balances for each slice are:

$$\frac{dya_k}{dt} = \frac{(Fr_{k-1}\cdot ya_{k-1} - Fr_k\cdot ya_k - (-r_{A,k})\cdot w_{cat})}{n_{t,k}} \quad (36)$$

$$\frac{dyb_k}{dt} = \frac{(Fr_{k-1}\cdot yb_{k-1} - Fr_k\cdot yb_k + [-(-r_{C,k}) - (-r_{D,k})]\cdot w_{cat})}{n_{t,k}} \quad (37)$$

$$\frac{dyc_k}{dt} = \frac{(Fr_{k-1}\cdot yc_{k-1} - Fr_k\cdot yc_k + [(-r_{B,k}) - (-r_{C,k})]\cdot w_{cat})}{n_{t,k}} \quad (38)$$

$$\frac{dyd_k}{dt} = \frac{(Fr_{k-1}\cdot yd_{k-1} - Fr_k\cdot yd_k + [(-r_{B,k}) + (-r_{C,k}) - (-r_{D,k})]\cdot w_{cat})}{n_{t,k}} \quad (39)$$

$$\frac{dye_k}{dt} = \frac{(Fr_{k-1}\cdot ye_{k-1} - Fr_k\cdot ye_k + (-r_{D,k})\cdot w_{cat})}{n_{t,k}} \quad (40)$$

$$\frac{dyf_k}{dt} = \frac{(Fr_{k-1}\cdot yf_{k-1} - Fr_k\cdot yf_k + [(-r_{A,k}) + 3(-r_{C,k}) + (-r_{D,k})]\cdot w_{cat})}{n_{t,k}} \quad (41)$$

$$\frac{dyg_k}{dt} = \frac{(Fr_{k-1}\cdot yg_{k-1} - Fr_k\cdot yg_k + [(-r_{A,k}) - (-r_{B,k})]\cdot w_{cat})}{n_{t,k}} \quad (42)$$

The energy balance gives the following differential equation for temperature variation:

$$\frac{dT_k}{dt} = \left(\frac{Fr_{k-1}\cdot cp_{k-1}\cdot T_{k-1} - Fr_k\cdot cp_k\cdot T_k + [(-r_{A,k})\cdot(-\Delta H_A) + (-r_{B,k})\cdot(-\Delta H_B) + (-r_{C,k})\cdot(-\Delta H_C) + (-r_{D,k})\cdot(-\Delta H_D)]\cdot w_{cat} + Q_k}{n_{t,k}\cdot cp_k}\right) \quad (43)$$

The energy balance for the ESR at the jacket side considers the heat exchanged with the internal part of the reactor where the main reaction occur. Since in the jacket there is no reaction, no component mass balance is needed, then only total mass balance must be considered:

$$\frac{dh_{gases(k)}}{dt} = F_{gases(k-1)} - F_{gases(k)} \quad (44)$$

Where $h_{gases(k)}$ is the holdup of gas in each slice. The gas temperature variation is obtained from the energy balance:

$$\frac{dT_{g(k)}}{dt} = \frac{\left(F_{gases(k-1)}\cdot cp_{gases(k-1)}\cdot T_{g(k-1)} - F_{gases(k)}\cdot cp_{gases(k)}\cdot T_{g(k)} - Q_k\right)}{h_{gases(k)}\cdot cp_{gases(k)}} \quad (45)$$

And $Q_k$ represents the heat exchanged, which is given by the algebraic expression:

$$Q_k = \frac{4}{Dt}\cdot(h_1\cdot D)_k\cdot V_{sl}\cdot(T_{g(k)} - T_k) \quad (46)$$

$(h_1\cdot D)_k$ is the warming correlation, given by [36]:

$$(h_1\cdot D)_k = 0.813\cdot Re^{0.9}\cdot\exp\left(-6\frac{Dp}{Dt}\right)\cdot k_{mix} \quad (47)$$

The gaseous mix thermal conductivity, $k_{mix}$, can be calculated by the expression of [37]:

$$k_{mix} = 0.01\frac{\sum_j y_j\cdot k_j\cdot M_j^{\frac{1}{3}}}{\sum_j y_j\cdot M_j^{\frac{1}{3}}} \quad (48)$$

The thermal conductivity of each component, $k_j$ is calculated using the Eucken approximation ([37]).

*Water gas shift*

Since both reactors have the same reaction scheme, the balances presented in this section are valid for both of them:

$$\frac{dn_{t,k}}{dt} = Fr_{k-1} - Fr_k = 0 \quad (49)$$

And the mass balances by component can be expressed as

$$\frac{dya_k}{dt} = \frac{(Fr_{k-1}\cdot ya_{k-1} - Fr_k\cdot ya_k)}{n_{t,k}} \quad (50)$$

$$\frac{dyb_k}{dt} = \frac{(Fr_{k-1}\cdot yb_{k-1} - Fr_k\cdot yb_k - (-r_{WGS,k})\cdot w_{cat})}{n_{t,k}} \quad (51)$$

$$\frac{dyc_k}{dt} = \frac{(Fr_{k-1}\cdot yc_{k-1} - Fr_k\cdot yc_k)}{n_{t,k}} \quad (52)$$

$$\frac{dyd_k}{dt} = \frac{(Fr_{k-1}\cdot yd_{k-1} - Fr_k\cdot yd_k - (-r_{WGS,k})\cdot w_{cat})}{n_{t,k}} \quad (53)$$

$$\frac{dye_k}{dt} = \frac{(Fr_{k-1}\cdot ye_{k-1} - Fr_k\cdot ye_k + (-r_{WGS,k})\cdot w_{cat})}{n_{t,k}} \quad (54)$$

$$\frac{dyf_k}{dt} = \frac{(Fr_{k-1}\cdot yf_{k-1} - Fr_k\cdot yf_k + (-r_{WGS,k})\cdot w_{cat})}{n_{t,k}} \quad (55)$$

$$\frac{dyg_k}{dt} = \frac{(Fr_{k-1}\cdot yg_{k-1} - Fr_k\cdot yg_k)}{n_{t,k}} \quad (56)$$

The energy balance for both reactors gives the temperature variation as:

$$\frac{dT_k}{dt} = \frac{Fr_{k-1}\cdot cp_{k-1}\cdot T_{k-1} - Fr_k\cdot cp_k\cdot T_k + (-r_{WGS,k})\cdot(-\Delta H_{WGS})\cdot w_{cat}}{n_{t,k}\cdot cp_k} \quad (57)$$

Since the reactors are considered adiabatic, there is no heat exchanged. Hence, all the heat produced during the reaction is used to raise the temperature of the stream.

*Preferential oxidation of carbon monoxide*

The total mass balance for this reactor can be expressed as follows:

$$\frac{dn_{t,k}}{dt} = Fr_{k-1} - Fr_k + \frac{1}{2}[-(-r_{E,k}) - (-r_{F,k})]\cdot w_{cat} = 0 \quad (58)$$

The reaction rates are based in CO and $H_2$, then the corresponding component mass balances are:

$$\frac{dya_k}{dt} = \frac{(Fr_{k-1}\cdot ya_{k-1} - Fr_k\cdot ya_k)}{n_{t,k}} \quad (59)$$

$$\frac{dyb_k}{dt} = \frac{(Fr_{k-1}\cdot yb_{k-1} - Fr_k\cdot yb_k + [(-r_{F,k}) - (-r_{WGS,k})]\cdot w_{cat})}{n_{t,k}} \quad (60)$$

$$\frac{dyc_k}{dt} = \frac{(Fr_{k-1}\cdot yc_{k-1} - Fr_k\cdot yc_k)}{n_{t,k}} \quad (61)$$

$$\frac{dyd_k}{dt} = \frac{(Fr_{k-1}\cdot yd_{k-1} - Fr_k\cdot yd_k + [-(-r_{E,k}) - (-r_{WGS,k})]\cdot w_{cat})}{n_{t,k}} \quad (62)$$

$$\frac{dye_k}{dt} = \frac{(Fr_{k-1}\cdot ye_{k-1} - Fr_k\cdot ye_k + [(-r_{E,k}) + (-r_{WGS,k})]\cdot w_{cat})}{n_{t,k}} \quad (63)$$

$$\frac{dyf_k}{dt} = \frac{(Fr_{k-1}\cdot yf_{k-1} - Fr_k\cdot yf_k + [-(-r_{F,k}) + (-r_{WGS,k})]\cdot w_{cat})}{n_{t,k}} \quad (64)$$

$$\frac{dyg_k}{dt} = \frac{(Fr_{k-1}\cdot yg_{k-1} - Fr_k\cdot yg_k)}{n_{t,k}} \quad (65)$$

$$\frac{dyh_k}{dt} = \frac{\left(Fr_{k-1}\cdot yh_{k-1} - Fr_k\cdot yh_k + \frac{1}{2}[-(-r_{E,k}) - (-r_{F,k})]\cdot w_{cat}\right)}{n_{t,k}} \quad (66)$$

From the energy balance the temperature variation is expressed as:

$$\frac{dT_k}{dt} = \left(\frac{Fr_{k-1}\cdot cp_{k-1}\cdot T_{k-1} - Fr_k\cdot cp_k\cdot T_k + [(-r_{WGS,k})\cdot(-\Delta H_{WGS}) + (-r_{E,k})\cdot(-\Delta H_E) + (-r_{F,k})\cdot(-\Delta H_F)]\cdot w_{cat}\cdot T_k}{n_{t,k}\cdot cp_k}\right) \quad (67)$$

Again, adiabatic reaction is considered so, all the heat generated from the reaction increases the temperature of the stream.

Although many publications present kinetic expressions for CO oxidation, only few of them consider the simultaneous $H_2$ oxidation. The work of [27] accounted both reactions and considered the WGS, with a Pt-Fe/$Al_2O_3$ catalyst

$$r_{CO} = 0.098\cdot\exp\left(-\frac{33092}{R_g\cdot T}\right)\cdot P_{CO}^{-0.1}\cdot P_{O_2}^{0.5} \quad (68)$$

$$r_{H_2} = 0.005703\cdot\exp\left(-\frac{18742}{R_g\cdot T}\right)\cdot P_{O_2}^{0.5} \quad (69)$$

$$r_{WGS} = 1.2227778\cdot\exp\left(-\frac{34104}{R_g\cdot T}\right)\cdot\left(P_{CO}\cdot P_{H_2O} - \frac{P_{CO_2}\cdot P_{H_2}}{K_{eq}}\right) \quad (70)$$

Where $K_{eq}$ can be calculated from Equation (8), and $P_j$ is the partial pressure of component $j$ (CO, $H_2O$, $CO_2$ and $H_2$).

*Burner*

The total mass balance is:

$$\frac{dn_t}{dt} = Fr_{in} - Fr_{out} + EtOH_{react} = 0 \quad (71)$$

And the component mass balances can be expressed as:

$$\frac{dya}{dt} = \frac{(Fr_{in}\cdot ya_{in} - Fr_{out}\cdot ya_{out} - EtOH_{react})}{n_t} \quad (72)$$

$$\frac{dyb}{dt} = \frac{(Fr_{in} \cdot yb_{in} - Fr_{out} \cdot yb_{out} + 3 \cdot EtOH_{react} + 2 \cdot CH_{4react})}{n_t} \quad (73)$$

$$\frac{dyc}{dt} = \frac{(Fr_{in} \cdot yc_{in} - Fr_{out} \cdot yc_{out} - CH_{4react})}{n_t} \quad (74)$$

$$\frac{dyd}{dt} = \frac{(Fr_{in} \cdot yd_{in} - Fr_{out} \cdot yd_{out})}{n_t} \quad (75)$$

$$\frac{dye}{dt} = \frac{(Fr_{in} \cdot ye_{in} - Fr_{out} \cdot ye_{out} + 2 \cdot EtOH_{react} + CH_{4react})}{n_t} \quad (76)$$

$$\frac{dyf}{dt} = \frac{(Fr_{in} \cdot yf_{in} - Fr_{out} \cdot yf_{out})}{n_t} \quad (77)$$

$$\frac{dyg}{dt} = \frac{(Fr_{in} \cdot yg_{in} - Fr_{out} \cdot yg_{out})}{n_t} \quad (78)$$

$$\frac{dyh}{dt} = \frac{(Fr_{in} \cdot yg_{in} - Fr_{out} \cdot yg_{out} - 3 \cdot EtOH_{react} - 2 \cdot CH_{4react})}{n_t} \quad (79)$$

From the energy balance for this reactor the temperature variation can be obtained by

$$\frac{dT}{dt} = \left( \frac{Fr_{in} \cdot cp_{in} \cdot T_{in} - Fr_{out} \cdot cp_{out} \cdot T_{out} + (EtOH_{react} \cdot \Delta H_{EtOH} + CH_{4react} \cdot \Delta H_{CH_4}) \cdot w_{cat}}{n_t \cdot cp_{out}} \right) \quad (80)$$

*Identified linear models*

**Table A1 – Abbreviations of used components.**

| | | |
|---|---|---|
| a | Ethanol | $CH_3CH_2OH$ |
| b | Water | $H_2O$ |
| c | Methane | $CH_4$ |
| d | Carbon Monoxide | CO |
| e | Carbon Dioxide | $CO_2$ |
| f | Hydrogen | $H_2$ |
| g | Acetaldehyde | $CH_3CHO$ |
| h | Oxygen | $O_2$ |

**Table A2 – Nomenclature.**

| Nomenclature | |
|---|---|
| nt | Accumulated moles in each slice |
| F | Reactor feed flow (mol/sec) |
| Fr | Exit flow in each slice (mol/sec) |
| $(-r_j)$ | Reaction rate (mol/*g*.sec) |
| $w_{cat}$ | Catalyst mass (*g*) |
| $y_i$ | Molar fraction of component i |
| cp | Mean specific heat (kj/mol × K) |
| T | Reactor temperature (K) |
| Tg | Hot gases chamber temperature (K) |
| $\Delta H_j$ | Reaction heat (kJ/mol) |
| $Fr_0$ | Nominal flow in each slice (mol/sec) |
| P | Pressure in each slice (Atm) |
| $\Delta P_0$ | Nominal pressure drop (Atm) |
| Pr | Products of the reaction |
| Rc | Reactants |
| Q | Exchanged heat flow (kg/sec) |
| $h_{gases}$ | Accumulated moles in hot gases chamber (mol) |
| $F_{gases}$ | Feed flow to hot gases chamber (mol/sec) |
| $cp_{gases}$ | Mean specific heat of hot gases (kJ/mol × K) |
| kj | Frequency factor (mol/*g* × sec) |
| Rg | Ideal gas constant (kJ/mol × K) |
| $\overline{R}$ | Ideal gas constant (j/kJ × K) |
| Ej | Activation energy (kJ/mol × K) |

**Table A2 – (*continued*)**

| Nomenclature | |
|---|---|
| $K_{eq}$ | Equilibrium constant |
| $h_1 \cdot D$ | Heat transmission coefficient (j/sec × $cm^2$ × K) |
| Dt | Tubular reactor diameter ($cm^2$) |
| $V_{sl}$ | Volume of each slice ($cm^3$) |
| Re | Reynolds for flow through packed bed |
| $D_p$ | Catalyst particle diameter (cm) |
| kmix | Gaseous mix conductivity (kj/sec × $cm^2$ × K) |
| t | Time (sec) |
| $\Delta g_f$ | Change in Gibbs free energy (J) |
| $\Delta S^0$ | Entropy variation (J/K) |

**Table A3 – Nomenclature.**

| Acronyms | |
|---|---|
| BPS | Bio-ethanol Processor System |
| PEM-FC | Proton Exchange Membrane – Fuel Cell |
| WGS | Water Gas Shift |
| CPO | Catalytic Partial Oxidation |
| ESR | Ethanol Steam Reforming |
| CO-PrOx | Preferential Oxidation of Carbon Monoxide |
| CSTR | Continuous Stirred Tank Reactors |
| HTS | High Temperature water gas Shift |
| LTS | Low Temperature water gas Shift |
| **Greek letters** | |
| $\alpha j$ | Reaction order |
| $\nu$ | Stoichiometric coefficient |
| **Subscripts** | |
| i | Reaction |
| j | Component |
| k | Slice |

**Table A4 – Matrix $\hat{A}$ from the SI.**

| | | | | | | | | | | | | | | |
|---|---|---|---|---|---|---|---|---|---|---|---|---|---|---|
| 0.0025 | 0.0220 | 0.0138 | −0.0001 | −0.0079 | −0.0007 | −0.0047 | −0.0166 | 0.0006 | −0.0081 | 0.0214 | 0.0048 | −0.0019 | −0.0160 | −0.0060 |
| 0.0443 | 0.2024 | 0.1307 | −0.0549 | −0.0258 | 0.0465 | −0.0256 | 0.0095 | −0.0004 | 0.0220 | −0.0024 | 0.0030 | 0.0008 | −0.0120 | −0.0034 |
| 0.2171 | 0.4800 | 0.4483 | 0.1003 | 0.0609 | −0.0224 | −0.0363 | 0.0017 | 0.0046 | −0.0295 | −0.0099 | 0.0123 | 0.0171 | 0.0194 | 0.0044 |
| 0.1601 | −0.1238 | 0.1770 | 0.2455 | 0.0955 | 0.0661 | 0.1361 | −0.0406 | −0.0218 | 0.0068 | 0.0162 | 0.0099 | −0.0019 | 0.0447 | 0.0253 |
| 0.1441 | −0.2183 | 0.1792 | 0.1293 | 0.4171 | −0.0227 | 0.0272 | 0.1839 | 0.0024 | −0.0192 | −0.0087 | −0.0029 | 0.0038 | −0.1194 | 0.0297 |
| 0.1118 | −0.5913 | −0.0671 | 0.1991 | 0.2170 | 0.2392 | 0.2133 | 0.0574 | −0.1369 | −0.0020 | 0.0913 | 0.0096 | −0.0245 | −0.0089 | −0.0545 |
| −0.0927 | 0.4062 | −0.4019 | 0.1212 | 0.2486 | 0.0498 | 0.5924 | 0.0788 | 0.0699 | −0.1988 | 0.1154 | 0.0099 | 0.0227 | 0.1462 | −0.0367 |
| 0.0228 | −0.0693 | −0.2250 | 0.1103 | 0.1173 | −0.7756 | −0.0977 | 0.4681 | −0.1074 | 0.0435 | 0.0576 | −0.0068 | 0.0827 | 0.0809 | −0.1344 |
| 0.0100 | −0.0239 | 0.4792 | −0.0495 | 0.0473 | 0.1263 | 0.1672 | 0.4631 | 0.5807 | 0.2070 | 0.0365 | −0.0360 | 0.0828 | −0.3449 | 0.0847 |
| −0.1217 | 0.1003 | −0.0263 | 0.1849 | 0.3400 | −0.4732 | 0.1228 | −0.4804 | 0.2678 | 0.2435 | 0.1618 | 0.1715 | −0.1907 | 0.5768 | −0.1145 |
| 0.0193 | 0.0540 | 0.2080 | −0.0397 | −0.0611 | −0.1595 | −0.0276 | −0.1147 | −0.3796 | 0.0142 | 0.8221 | 0.1395 | 0.2174 | −0.2248 | 0.0450 |
| 0.0840 | −0.0090 | 0.0673 | −0.0029 | 0.2305 | 0.0077 | −0.1439 | −0.0153 | −0.0823 | −0.2750 | 0.0428 | 0.9370 | 0.0474 | 0.1496 | −0.0160 |
| 0.1120 | −0.2153 | 0.1640 | 0.2439 | −0.1973 | 0.0056 | 0.0027 | −0.3218 | 0.1930 | 0.2271 | −0.2102 | −0.1868 | 0.5867 | 0.0736 | −0.1452 |
| −0.0164 | 0.0561 | −0.1922 | 0.0263 | 0.1601 | 0.1232 | −0.4032 | 0.2302 | 0.0935 | −0.0953 | 0.3276 | −0.1843 | 0.0755 | 1.0103 | 0.0411 |
| −0.0807 | 0.1790 | −0.1929 | 0.1318 | 0.2816 | 0.1069 | −0.3008 | 0.0509 | −0.0430 | 0.3921 | −0.3205 | 0.0295 | 0.2532 | −0.3866 | 0.8413 |

**Table A5 – Matrix $\hat{B}$ from the SI.**

| | | | | | | | |
|---|---|---|---|---|---|---|---|
| 0.0188 | −0.0001 | 0.0106 | 0.1111 | 0.0012 | −0.0001 | 0.0100 | −0.0017 |
| −0.0177 | −0.0734 | 0.0044 | −0.0013 | −0.0025 | −0.0057 | −0.0100 | 0.0001 |
| 0.0225 | 0.0653 | −0.0109 | −0.0478 | 0.0014 | −0.0270 | 0.0111 | −0.0006 |
| −0.0446 | 0.0264 | −0.0383 | 0.0049 | 0.0020 | −0.0172 | −0.0463 | 0.0104 |
| −0.0520 | −0.0342 | 0.0506 | −0.0310 | −0.0050 | −0.0030 | 0.0303 | −0.0244 |
| 0.0893 | −0.0747 | −0.0040 | −0.0154 | 0.0007 | −0.0112 | −0.0368 | 0.0011 |
| 0.0411 | 0.0386 | −0.0286 | 0.0030 | −0.0059 | 0.0100 | 0.0233 | −0.0173 |
| 0.0873 | −0.0162 | −0.0331 | −0.0122 | 0.0009 | −0.0185 | −0.0069 | −0.0006 |
| −0.0165 | −0.0265 | 0.0289 | 0.0323 | 0.0125 | 0.0413 | −0.0368 | 0.0194 |
| 0.1092 | −0.0160 | −0.0464 | 0.0232 | −0.0240 | 0.0245 | −0.0077 | −0.0273 |
| 0.0187 | −0.0173 | 0.0053 | 0.0189 | 0.0040 | 0.0280 | −0.0160 | −0.0107 |
| 0.0361 | −0.0201 | −0.0248 | 0.0132 | −0.0088 | 0.0389 | −0.0108 | −0.0119 |
| −0.0334 | −0.0384 | 0.0113 | −0.0256 | 0.0040 | 0.0074 | 0.0481 | 0.0145 |
| 0.0099 | 0.0086 | −0.0217 | −0.0012 | −0.0092 | 0.0065 | 0.0121 | −0.0067 |
| 0.0258 | 0.0138 | −0.0109 | 0.0124 | 0.0159 | 0.0075 | 0.0064 | 0.0012 |

**Table A6 – Matrix $\hat{C}$ from the SI.**

| | | | | | | | | | | | | | | |
|---|---|---|---|---|---|---|---|---|---|---|---|---|---|---|
| 1.4689 | −8.9408 | 0.3345 | 2.9181 | 1.0139 | 1.6417 | −2.3280 | −2.6402 | −0.9431 | 1.2071 | 2.3949 | −1.4676 | 0.4727 | 1.3244 | 0.5625 |
| 5.4537 | 5.1850 | −1.1802 | 3.8667 | 0.8057 | 4.4253 | −1.2400 | −5.4667 | −2.5689 | 2.0509 | 5.1993 | −2.6765 | 1.8574 | 2.9381 | 1.7294 |
| −3.6164 | 0.8794 | 1.1102 | −7.2542 | 4.1996 | −3.3688 | 3.0260 | 3.7737 | 4.2011 | 0.0230 | −5.8333 | 1.1671 | −1.8935 | −6.1374 | −1.1511 |
| 0.5678 | −0.2175 | 1.7156 | −6.5987 | −2.8459 | −2.0156 | 0.3584 | 6.2047 | 2.9314 | −1.7073 | −4.7741 | 2.2296 | −1.3634 | −1.9106 | −2.3421 |
| 0.9967 | −2.3281 | 1.3006 | 2.4486 | 1.4961 | 4.5420 | 0.1081 | −5.4769 | −2.5742 | 1.4661 | 4.3595 | −1.9557 | 1.8827 | 1.7182 | 2.1473 |
| 0.2680 | −6.0950 | −3.3297 | 5.3724 | 4.3614 | 0.7903 | −1.2556 | 0.6578 | −0.5240 | 0.3878 | 0.8860 | −0.2057 | 0.6936 | −0.1973 | 0.1890 |
| −0.4780 | −0.7079 | −4.5277 | −0.0675 | 3.7953 | −2.4794 | 5.5456 | 6.3550 | 2.5032 | −3.1558 | −13.5734 | 9.3865 | −3.4085 | −11.8763 | 1.5109 |
| −1.2391 | 0.7795 | −2.9203 | 5.7293 | 5.3909 | −0.4808 | 6.6240 | 0.2934 | 2.1613 | 0.0512 | −5.5291 | 2.5212 | 0.2033 | −7.4412 | 3.3845 |
| 0.3890 | −0.2608 | 3.5541 | 0.7920 | −3.7987 | 3.3078 | −6.4066 | −7.8361 | −4.2586 | 2.5652 | 14.2083 | −7.6724 | 3.5477 | 11.3886 | −1.1234 |
| 8.4947 | 0.4436 | 0.0418 | −0.2537 | −0.8502 | −0.8066 | −0.8478 | 0.3829 | 0.2602 | −0.0012 | 0.7765 | −0.6034 | −0.0216 | 1.0373 | −0.7370 |
| −0.2166 | −1.0454 | −3.0250 | −1.8449 | 0.8582 | −1.3385 | 1.2344 | 4.0911 | 0.2433 | −2.5660 | −7.2662 | 5.4123 | −2.9828 | −5.4069 | 0.1478 |
| −8.9110 | −15.6145 | −22.8989 | −4.2992 | −4.0485 | 2.7966 | 3.7678 | −1.7149 | −6.2327 | −3.4327 | −0.0629 | −1.8012 | −3.3380 | −1.5469 | −0.3408 |
| −3.2666 | −5.1972 | −5.7284 | −1.3961 | −0.6287 | −1.0319 | 0.0440 | 0.3677 | 1.4528 | 0.8356 | 0.3553 | 0.4980 | 0.6563 | 0.2283 | 0.2336 |
| −2.1220 | −4.0126 | −6.5932 | −0.9493 | −1.1914 | 1.6036 | 1.4282 | −0.8519 | −2.9181 | −1.4215 | 0.0197 | −1.2158 | −1.3519 | −0.4790 | −0.1185 |

**Table A7 – Matrix $\hat{D}$ from the SI.**

| | | | | | | | |
|---|---|---|---|---|---|---|---|
| −0.0115 | 0.0160 | 0.0157 | −0.0220 | −0.0258 | −0.0281 | −0.0066 | 0.0180 |
| −0.0138 | 0.0085 | 0.0154 | −0.0041 | 0.0401 | −0.0253 | −0.0134 | 0.0239 |
| −0.0126 | 0.0080 | 0.0289 | −0.0094 | 0.0107 | −0.0162 | −0.0177 | 0.0251 |
| 0.0008 | −0.0080 | −0.0027 | 0.0065 | 0.0393 | 0.0021 | 0.0067 | 0.0114 |
| 0.5316 | 0.0046 | −0.0090 | 0.0036 | −0.0009 | −0.0003 | 0.0071 | −0.0116 |
| 0.0032 | −0.0077 | −0.0081 | 0.0011 | −0.0032 | 0.0050 | 0.0077 | −0.0066 |
| −0.0201 | 0.0141 | 0.0046 | −0.0175 | −0.0268 | −0.0168 | 0.0081 | 0.0090 |
| 0.0736 | −0.0657 | −0.0162 | 0.1426 | 0.3092 | 0.1187 | −0.0022 | −0.0191 |
| −0.0097 | 0.0215 | −0.0028 | 0.0044 | 0.2273 | −0.0287 | −0.0092 | 0.0095 |
| −0.0041 | 0.0056 | 0.0004 | −0.0054 | −0.0096 | −0.0053 | 0.0020 | 0.0007 |
| −0.0814 | 0.0627 | 0.0376 | −0.0947 | −0.0799 | −0.1321 | −0.0475 | 0.0672 |
| 0.0017 | −0.0059 | −0.0157 | 0.0245 | 0.0061 | −2.0195 | 0.0755 | 1.0151 |
| −0.0062 | 0.0019 | −0.0026 | −0.0068 | 0.0034 | −0.0164 | −0.0104 | −0.5967 |
| 0.0020 | −0.0028 | −0.0016 | 0.0045 | 0.0007 | 0.0149 | 0.0211 | −0.7013 |

## REFERENCES


[1] Momirlan M, Veziroglu T. The properties of hydrogen as fuel tomorrow in sustainable energy system for a cleaner planet. International Journal of Hydrogen Energy 2005;30(7):795–802.

[2] Aicher T, Full J, Schaadt A. A portable fuel processor for hydrogen production from ethanol in a 250wel fuel cell system. International Journal of Hydrogen Energy 2009; 34(19):8006–15.

[3] Sanchez OJ, Cardona CA. Producción biotecnológica de alcohol carburante i: obtención a partir de diferentes materias primas. INCI 2005;30(11):671–8.

[4] Prakash R, Henham A, Krishnan Bhat I. Net energy and gross pollution from bioethanol production in india. Fuel 1998; 77(14):1629–33.

[5] Song H, Ozkan US. Economic analysis of hydrogen production through a bio-ethanol steam reforming process: sensitivity analyses and cost estimations. International Journal of Hydrogen Energy 2010;35(1):127–34.

[6] Gregorini VA, Pasquevich D, Laborde M. Price determination for hydrogen produced from bio-ethanol in argentina. International Journal of Hydrogen Energy 2010;35(11):5844–8.

[7] Oakley JH, Hoadley AF. Industrial scale steam reforming of bioethanol: a conceptual study. International Journal of Hydrogen Energy 2010;35(16):8472–85.

[8] Jalowiecki-Duhamel L, Pirez C, Capron M, Dumeignil F, Payen E. Hydrogen production from ethanol steam reforming over cerium and nickel based oxyhydrides. International Journal of Hydrogen Energy 2010;35(23): 12741–12750s.

[9] Manzolini G, Tosti S. Hydrogen production from ethanol steam reforming: energy efficiency analysis of traditional and membrane processes. International Journal of Hydrogen Energy 2008;33(20):5571–82.

[10] Fogler HS. Elements of chemical reaction Engineering. 4th ed. Prentice-Hall PTR; 2005.

[11] Oliva DG, Francesconi JA, Mussati MC, Aguirre PA. Modeling, synthesis and optimization of heat exchanger networks. Application to fuel processing systems for pem fuel cells. International Journal of Hydrogen Energy 2011;36(15): 9098–114.

[12] Boehme TR, Onder CH, Guzzella L. Dynamic model of an auto-thermal gasoline fuel processor. International Journal of Hydrogen Energy 2008;33(21):6150–64.

[13] Parvasi P, Mostafazadeh AK, Rahimpour M. Dynamic modeling and optimization of a novel methanol synthesis loop with hydrogen-permselective membrane reactor. International Journal of Hydrogen Energy 2009;34(9):3717–33.

[14] Koc R, Kazantzis NK, Ma YH. A process dynamic modeling and control framework for performance assessment of pd/alloy-based membrane reactors used in hydrogen production. International Journal of Hydrogen Energy 2011; 36(8):4934–51.

[15] Pukrushpan JT, Stefanopoulou A, Varigonda S, Eborn J, Haugstetter C. Control-oriented model of fuel processor for hydrogen generation in fuel cell applications. Control Engineering Practice 2003;14(3):277–93.

[16] Varigonda S, Pukrushpan JT, Stefanopoulou A. Challenges in fuel cell power plant control: the role of system level dynamic models. IEEE Transactions on Control Systems Technology 2003;13(1):3–14.

[17] Pukrushpan JT, Stefanopoulou A, Varigonda S, Pedersen LM, Ghosh S, Peng H. Control of natural gas catalytic partial oxidation for hydrogen generation in fuel cell applications. IEEE Transactions on Control Systems Technology 2003;13(1): 3–14.

[18] Chuang CC, Cheng YH, Ward JD, Yu CC, Liu YC, Lee CH. Optimal design of an experimental methanol fuel reformer. International Journal of Hydrogen Energy 2008; 33:7062–73.

[19] Francesconi J, Mussati M, Mato R, Aguirre P. Analysis of the energy efficiency of an integrated ethanol processor for PEM fuel cell systems. Journal of Power Sources 2007;167(1): 151–61.

[20] Pukrushpan JT, Stephanopoulou AG, Peng H. Control of fuel cell power systems: principles, modeling, analysis, and feedback design. Springer; 2004.

[21] Biset S, Degliuomini LN, Basualdo M, Garcia V, Serra M. Analysis of the control structures for an integrated ethanol processor for proton exchange membrane fuel cell systems. Journal of Power Sources 2009;192(1):107–13.

[22] Poling BE, Prausnitz JM, O'Connell JP. The Properties of gases and liquids. 5th ed. New York: McGraw-Hill; 2000.

[23] Francesconi JA, Modelado, síntesis y optimización del proceso de reformado de bioetanol para la producción de hidrógeno grado pem, Ph.D. thesis, Universidad Nacional del Litoral (2008).

[24] Benito M, Sanz J, Isabel R, Padilla R, Arjona R, Daza L. Bio-ethanol steam reforming: insights on the mechanism for hydrogen production. Journal of Power Sources 2005;151: 11–7.

[25] Keiski RL, Salmi T, Pohjola VJ. Development and verification of a simulation model for a non-isothermal water-gas shift reactor. Chem. Eng. J 1992;48(1):17–29.

[26] Choi Y, Stenger HG. Water gas shift reaction kinetics and reactor modeling for fuel cell grade hydrogen. Journal of Power Sources 2003;124(2):432–9.

[27] Choi Y, Stenger HG. Kinetics, simulation and insights for CO selective oxidation in fuel cell applications. J. Power Sources 2004;129(2):246–54.
[28] Larminie J, Dicks A. Fuel cell power systems explained. West Sussex, England: John Wiley & Sons Inc; 2000.
[29] Grujicic M, Chittajallu K, Law E, Pukrushpan J. Model-based control strategies in the dynamic interaction of air supply and fuel cell, proceedings of the institution of mechanical engineers, part A. Journal of Power and Energy 2004;218(7):487–99.
[30] Luyben ML, Luyben WL. Essentials of process control. McGraw-Hill Chemical Engineering Series, International Editions; 1997.
[31] Linnhoff B, Townsend P, Boland P, Hewitt GF, Thomas BEA, Guy AR, et al. A user guide on process integration for the efficient use of energy, rev sub Edition. Rugby, UK: Institute of Chemical Engineers; 1994.
[32] Van Overschee P, De Moor B. N4SID: subspace algorithms for the identification of combined deterministic-stochastic systems. Automatica 1994;30:75–93.
[33] Ljung L. System identification (Theory for the user). 2nd ed.; 1999.
[34] Ljung L. System identification toolbox (user's guide version 5). Tech. rep., The Math Works Inc.; 2002.
[35] Rivera DE. Una metodología para la identificación integrada con el diseño de controladores IMC-PID. Revista Iberoamericana de Automática e Informática Industrial 2007; 4(4):129–34.
[36] Leva M, Weintraub M, Grummer M, Clarke EL. Cooling of gases flowing in turbulent motion through packed tubes. Industrial and Engineering Chemistry 1948;40:747–52.
[37] Perry RH, Chilton CH. Chemical engineering handbook. New York: McGraw-Hill; 1973.